Monotonicity in inverse obstacle scattering on unbounded domains

Annalena Albicker, Roland Griesmaier

KARLSRUHE INSTITUTE OF TECHNOLOGY

CRC 1173

Participating universities

Universität Stuttgart

EBERHARD KARLS
UNIVERSITÄT
TÜBINGEN

TU
WIEN

Funded by

DFG

Monotonicity in inverse obstacle scattering on unbounded domains

Annalena Albicker and Roland Griesmaier*

March 11, 2020

Abstract

We consider an inverse obstacle scattering problem for the Helmholtz equation with obstacles that carry mixed Dirichlet and Neumann boundary conditions. We discuss far field operators that map superpositions of plane wave incident fields to far field patterns of scattered waves, and we derive monotonicity relations for the eigenvalues of suitable modifications of these operators. These monotonicity relations are then used to establish a novel characterization of the support of mixed obstacles in terms of the corresponding far field operators. We apply this characterization in reconstruction schemes for shape detection and object classification, and we present numerical results to illustrate our theoretical findings.

1 Introduction

We discuss an inverse obstacle scattering problem for time-harmonic scalar waves governed by the Helmholtz equation. The goal is to recover the position and the shape of a collection of compactly supported scattering objects from far field observations of scattered waves. We consider impenetrable obstacles with mixed Dirichlet and Neumann boundary conditions, i.e., we assume that the scatterers $D = D_1 \cup D_2$ consist of two components such that $\overline{D_1} \cap \overline{D_2} = \emptyset$, where ∂D_1 carries a Dirichlet boundary condition while ∂D_2 carries a Neumann boundary condition. The Dirichlet part D_1 and the Neumann part D_2 of the scattering objects might consist of several connected components, and we do neither assume that the number of connected components nor whether they carry Dirichlet or Neumann boundary conditions are known a priori. Accordingly, qualitative reconstruction schemes (see, e.g., [3, 6, 9, 8, 30, 31, 35]), which do not make use of topological or physical properties of the scattering objects, are a natural choice. In addition to shape reconstruction, we will also show that the type of boundary condition on each connected component of the obstacle can be classified from scattering data, i.e., we show that the Dirichlet part D_1 and the Neumann part D_2 can be recovered separately.

Among qualitative methods for shape reconstruction, the linear sampling method has been successfully applied to inverse mixed obstacle scattering problems (see, e.g., [3, 4, 5]). The factorization

---

*Institut für Angewandte und Numerische Mathematik, Karlsruher Institut für Technologie, Englerstr. 2, 76131 Karlsruhe, Germany (`annalena.albicker@kit.edu`, `roland.griesmaier@kit.edu`).

method has been justified under the additional assumption that the Dirichlet part D_1 and the Neumann part D_2 of the scattering object can be separated a priori (see [18, 19, 31]). We build on and extend ideas from these works to develop a monotonicity based qualitative shape reconstruction technique. This *monotonicity method* is formulated in terms of far field operators that map superpositions of incident plane waves, which are being scattered at the unknown scattering objects, to the far field patterns of the corresponding scattered waves. It exploits monotonicity properties of the eigenvalues of suitable modifications of these operators. The main result of this work is a rigorous characterization of the support of mixed scattering obstacles in terms of the corresponding far field operators without any additional a priori information. This is a significant extension of the results in [18, 19, 31].

The monotonicity based approach to shape reconstruction has originally been developed for the inverse conductivity problem in [14, 26], extending an earlier monotonicity based reconstruction scheme developed in [37]. The method is related to monotonicity principles for the Laplace equation established in [28, 29]. It has been further developed in [22, 23, 27], its numerical implementation has been studied in [11, 12, 13], and recently an extension to impenetrable conductivity inclusions has been established in [7].

The analysis in [26] has been extended to inverse coefficient problems for the Helmholtz equation on bounded domains in [24, 25], and in [16] the approach has been generalized to the inverse medium scattering problem on unbounded domains with plane wave incident fields and far field observations of scattered waves. An application of the monotonicity method to an inverse crack detection problem for the Helmholtz equation has recently been considered in [10]. For further recent contributions on monotonicity based reconstruction methods for various inverse problems for partial differential equations we refer to [1, 2, 20, 21, 32, 36, 38].

The main idea of the monotonicity method for inverse mixed obstacle scattering that we discuss in this work, is to compare the real part of the given (or observed) far field operator corresponding to the unknown scattering obstacles to various virtual (or simulated) probing operators corresponding to certain probing domains. We show that suitable linear combinations of these operators are positive definite up to a finite dimensional subspace if and only if the probing domains are contained inside the support of the scattering objects or if and only if the probing domains contain the unknown scattering object. This can be translated into criteria and algorithms for shape reconstruction.

This article is organized as follows. In Section 2 we briefly recall the mathematical formulation of the mixed obstacle scattering problem, and in Section 3 we discuss a factorization of the corresponding far field operator from [18, 19, 31]. In Section 4 we establish the existence of localized wave functions for the mixed obstacle scattering problem, and in Section 5 we use these localized wave functions to prove a rigorous characterization of the support of scattering obstacles in terms of the far field operator. We discuss numerical algorithms based on these theoretical results in Section 6, and we close with some concluding remarks.

2 Scattering by impenetrable obstacles

We consider the scattering of time-harmonic scalar waves in an unbounded homogeneous background medium by a collection of impenetrable obstacles carrying Dirichlet and Neumann boundary conditions. Suppose that $D = D_1 \cup D_2 \subseteq \mathbb{R}^d$, $d = 2, 3$, is open and Lipschitz bounded with connected complement $\mathbb{R}^d \setminus \overline{D}$ such that $\overline{D_1} \cap \overline{D_2} = \emptyset$. The subsets D_1 and D_2 may consist of finitely many connected components. Below we will impose Dirichlet boundary conditions on D_1 and Neumann

boundary conditions on D_2, and thus we refer to D_1 and D_2 as the *Dirichlet* and *Neumann obstacles*, respectively.

We assume that the wave motion is caused by an *incident field* $u^i \in H^1_{\text{loc}}(\mathbb{R}^d)$ satisfying the Helmholtz equation

$$\Delta u^i + k^2 u^i = 0 \qquad \text{in } \mathbb{R}^d \tag{2.1}$$

with *wave number* $k > 0$ that is being scattered at the *obstacle D*. The *scattered field* $u^s \in H^1_{\text{loc}}(\mathbb{R}^d)$ satisfies

$$\Delta u^s + k^2 u^s = 0 \qquad \text{in } \mathbb{R}^d \setminus \overline{D} \tag{2.2a}$$

and the boundary conditions

$$u^s = -u^i \quad \text{on } \partial D_1 \qquad \text{and} \qquad \frac{\partial u^s}{\partial \nu} = -\frac{\partial u^i}{\partial \nu} \quad \text{on } \partial D_2 \tag{2.2b}$$

together with the *Sommerfeld radiation condition*

$$\lim_{r \to \infty} r^{\frac{d-1}{2}} \left(\frac{\partial u^s}{\partial r}(x) - \mathrm{i}k u^s(x) \right) = 0, \qquad r = |x|, \tag{2.2c}$$

uniformly with respect to all directions $\widehat{x} := x/|x| \in S^{d-1}$. Throughout, the Helmholtz equation is to be understood in weak sense, but standard interior regularity results yield smoothness of u^s in $\mathbb{R}^d \setminus \overline{D}$. In particular the Sommerfeld radiation condition (2.2c) is well defined. As usual, we call a (weak) solution to a Helmholtz equation on an unbounded domain that satisfies the Sommerfeld radiation condition uniformly with respect to all directions a *radiating solution*.

Lemma 2.1. *Let $f \in H^{\frac{1}{2}}(\partial D_1)$ and $g \in H^{-\frac{1}{2}}(\partial D_2)$. Then the* exterior mixed boundary value problem

$$\Delta w + k^2 w = 0 \qquad \qquad \text{in } \mathbb{R}^d \setminus (\overline{D_1 \cup D_2}), \tag{2.3a}$$

$$w = f \qquad \qquad \text{on } \partial D_1, \tag{2.3b}$$

$$\frac{\partial w}{\partial \nu} = g \qquad \qquad \text{on } \partial D_2, \tag{2.3c}$$

has a unique radiating solution $w \in H^1_{\text{loc}}(\mathbb{R}^d)$.

Furthermore, the solution has the asymptotic behavior

$$w(x) = C_d \frac{e^{\mathrm{i}k|x|}}{|x|^{\frac{d-1}{2}}} w^\infty(\widehat{x}) + O(|x|^{-\frac{d+1}{2}}), \qquad |x| \to \infty,$$

uniformly in all directions $\widehat{x} \in S^{d-1}$, where

$$C_d = e^{\mathrm{i}\pi/4}/\sqrt{8\pi k} \quad \text{if } d = 2 \qquad \text{and} \qquad C_d = 1/(4\pi) \quad \text{if } d = 3, \tag{2.4}$$

and $w^\infty \in L^2(S^{d-1})$ is called the far field pattern *of w.*

Proof. The unique solvability follows, e.g., immediately from [31, Thm. 3.1] (see also [33, p. 288]), and the far field asymptotics are, e.g., shown in [9, Thm. 2.6]. $\square$

Choosing $f = -u^i|_{\partial D_1}$ and $g = -\partial u^i/\partial\nu|_{\partial D_2}$ in Lemma 2.1 proves the existence and unique-ness of solutions to the scattering problem (2.2). For the special case of a *plane wave incident field* $u^i(x;\theta) := e^{ikx\cdot\theta}$, $x \in \mathbb{R}^d$, we explicitly indicate the dependence on the *incident direc-tion* $\theta \in S^{d-1}$ by a second argument, and accordingly we write $u^s(\,\cdot\,;\theta)$, and $u^\infty(\,\cdot\,;\theta)$ for the corresponding scattered field and its far field pattern, respectively.

We define the *far field operator*

$$F_D^{\mathrm{mix}} : L^2(S^{d-1}) \to L^2(S^{d-1}), \quad (F_D^{\mathrm{mix}}g)(\widehat{x}) := \int_{S^{d-1}} u^\infty(\widehat{x};\theta)g(\theta)\,\mathrm{d}s(\theta), \qquad (2.5)$$

and we note that F_D^{mix} is compact and normal (see, e.g., [31, Thm. 3.3]). Moreover, the *scattering operator* is defined by

$$\mathcal{S}_D^{\mathrm{mix}} : L^2(S^{d-1}) \to L^2(S^{d-1}), \quad \mathcal{S}_D^{\mathrm{mix}}g := (I + 2\mathrm{i}k|C_d|^2 F_D^{\mathrm{mix}})g,$$

where C_d is again the constant from (2.4). The operator $\mathcal{S}_D^{\mathrm{mix}}$ is unitary, and consequently the eigenvalues of F_D^{mix} lie on the circle of radius $1/(2k|C_d|^2)$ centered in $\mathrm{i}/(2k|C_d|^2)$ in the complex plane (cf., e.g., [31, Thm. 3.3]).

Remark 2.2. In the special case when $D_2 = \emptyset$, i.e., when only Dirichlet obstacles are present, (2.3) reduces to the *exterior Dirichlet boundary value problem*, and we denote the corresponding far field operator by $F_{D_1}^{\mathrm{dir}}$. Similarly, if $D_1 = \emptyset$, i.e., when only Neumann obstacles are present, then (2.3) reduces to the *exterior Neumann boundary value problem*, and we denote the corresponding far field operator by $F_{D_2}^{\mathrm{neu}}$. $\diamondsuit$

3 Factorizations of the far field operator

Next we briefly recall three factorizations of the far field operators F_D^{mix}, $F_{D_1}^{\mathrm{dir}}$, and $F_{D_2}^{\mathrm{neu}}$, which have been used in the traditional factorization method, and that will be applied to develop the monotonicity based shape characterization in Section 5 below. As usual, the *single layer operator* is defined by

$$S_{D_1} : H^{-\frac{1}{2}}(\partial D_1) \to H^{\frac{1}{2}}(\partial D_1), \quad (S_{D_1}\varphi)(x) := \int_{\partial D_1} \Phi_k(x,y)\varphi(y)\,\mathrm{d}s(y), \qquad (3.1)$$

and the *normal derivative of the double layer potential* is given by

$$N_{D_2} : H^{\frac{1}{2}}(\partial D_2) \to H^{-\frac{1}{2}}(\partial D_2), \quad (N_{D_2}\psi)(x) := \frac{\partial}{\partial\nu}\int_{\partial D_2}\frac{\partial\Phi_k}{\partial\nu(y)}(x,y)\psi(y)\,\mathrm{d}s(y). \qquad (3.2)$$

Here, Φ_k denotes the fundamental solution to the Helmholtz equation in $\mathbb{R}^d$.

Remark 3.1. Throughout we denote by $\langle\cdot,\cdot\rangle$ the sesquilinear dual pairing between $H^{-\frac{1}{2}}(\partial D_j)$ and $H^{\frac{1}{2}}(\partial D_j)$, $j = 1,2$, which extends the inner product on $L^2(\partial D_j)$. $\diamondsuit$

3.1 Dirichlet or Neumann obstacles

The first result describes the factorization of the far field operator for Dirichlet obstacles.

4

Theorem 3.2. *(a) The far field operator $F_{D_1}^{\text{dir}} : L^2(S^{d-1}) \to L^2(S^{d-1})$ can be decomposed as*

$$F_{D_1}^{\text{dir}} = -G_{D_1}^{\text{dir}} S_{D_1}^* G_{D_1}^{\text{dir}*}, \tag{3.3}$$

where $G_{D_1}^{\text{dir}} : H^{\frac{1}{2}}(\partial D_1) \to L^2(S^{d-1})$ maps $f \in H^{\frac{1}{2}}(\partial D_1)$ to the far field pattern w^∞ of the unique radiating solution to the exterior Dirichlet boundary value problem (2.3a) and (2.3b).

(b) $G_{D_1}^{\text{dir}}$ is compact and one-to-one with dense range in $L^2(S^{d-1})$.

(c) If k^2 is not a Dirichlet eigenvalue of $-\Delta$ in D_1, then S_{D_1} is an isomorphism.

(d) Let $S_{D_1,\text{i}}$ be the single layer operator (3.1) corresponding to the wave number $k = \text{i}$. Then $S_{D_1,\text{i}}$ is self-adjoint and coercive, i.e., there exists $c_1 > 0$ such that

$$\langle \varphi, S_{D_1,\text{i}}\varphi \rangle \geq c_1 \|\varphi\|^2_{H^{-\frac{1}{2}}(\partial D_1)} \qquad \text{for all } \varphi \in H^{-\frac{1}{2}}(\partial D_1).$$

(e) The difference $S_{D_1} - S_{D_1,\text{i}}$ is compact.

Proof. This is shown in [31, Lmms. 1.13–1.14 and Thm. 1.15]. $\qquad\square$

Remark 3.3. An immediate consequence of Theorem 3.2 is that the real part[1]

$$-\operatorname{Re}(F_{D_1}^{\text{dir}}) = \frac{1}{2} G_{D_1}^{\text{dir}}(S_{D_1} + S_{D_1}^*) G_{D_1}^{\text{dir}*}$$

is a compact perturbation of a self-adjoint and coercive operator. This implies that $\operatorname{Re}(F_{D_1}^{\text{dir}})$ has only finitely many positive eigenvalues. In Theorem 5.3 below we will significantly refine and extend this observation. $\qquad\diamond$

Next we consider the factorization of the far field operator for Neumann obstacles.

Theorem 3.4. *(a) The far field operator $F_{D_2}^{\text{neu}} : L^2(S^{d-1}) \to L^2(S^{d-1})$ can be decomposed as*

$$F_{D_2}^{\text{neu}} = -G_{D_2}^{\text{neu}} N_{D_2}^* G_{D_2}^{\text{neu}*},$$

where $G_{D_2}^{\text{neu}} : H^{-\frac{1}{2}}(\partial D_2) \to L^2(S^{d-1})$ maps $g \in H^{-\frac{1}{2}}(\partial D_2)$ to the far field pattern w^∞ of the unique radiating solution to the exterior Neumann boundary value problem (2.3a) and (2.3c).

(b) $G_{D_2}^{\text{neu}}$ is compact and one-to-one with dense range in $L^2(S^{d-1})$.

(c) If k^2 is not a Neumann eigenvalue of $-\Delta$ in D_2, then N_{D_2} is an isomorphism.

(d) Let $N_{D_2,\text{i}}$ be the normal derivative of the double layer potential (3.2) corresponding to the wave number $k = \text{i}$. Then $-N_{D_2,\text{i}}$ is self-adjoint and coercive, i.e., there exists $c_2 > 0$ such that

$$-\langle N_{D_2,\text{i}}\psi, \psi \rangle \geq c_2 \|\psi\|^2_{H^{\frac{1}{2}}(\partial D_2)} \qquad \text{for all } \psi \in H^{\frac{1}{2}}(\partial D_2).$$

(e) The difference $N_{D_2} - N_{D_2,\text{i}}$ is compact.

---

[1] As usual the real part of a linear operator $A : X \to X$ on a Hilbert space X is the self-adjoint operator given by $\operatorname{Re}(A) := \frac{1}{2}(A + A^*)$.

Proof. This is shown in [31, Thm. 1.26]. □

Remark 3.5. An immediate consequence of Theorem 3.4 is that the real part

$$\mathrm{Re}(F_{D_2}^{\mathrm{neu}}) \, = \, -\frac{1}{2}G_{D_2}^{\mathrm{neu}}(N_{D_2} + N_{D_2}^*)G_{D_2}^{\mathrm{neu}*}$$

is a compact perturbation of a self-adjoint and coercive operator. This implies that $\mathrm{Re}(F_{D_2}^{\mathrm{neu}})$ has only finitely many negative eigenvalues. In Theorem 5.4 below we will significantly refine and extend this observation. ◇

3.2 Mixed obstacles

In the mixed case the obstacle $D = D_1 \cup D_2$ consists of two bounded components and carries Dirichlet boundary conditions on ∂D_1 and Neumann boundary conditions on ∂D_2.

Theorem 3.6. *(a) The far field operator* $F_D^{\mathrm{mix}} : L^2(S^{d-1}) \to L^2(S^{d-1})$ *can be decomposed as*

$$F_D^{\mathrm{mix}} \, = \, -G_D^{\mathrm{mix}}T_D^{\mathrm{mix}*}G_D^{\mathrm{mix}*}\,,$$

where $G_D^{\mathrm{mix}} : H^{\frac{1}{2}}(\partial D_1) \times H^{-\frac{1}{2}}(\partial D_2) \to L^2(S^{d-1})$ *maps* $(f,g) \in H^{\frac{1}{2}}(\partial D_1) \times H^{-\frac{1}{2}}(\partial D_2)$ *to the far field pattern* w^∞ *of the unique radiating solution to the exterior mixed boundary value problem* (2.3a)–(2.3c). *The operator* $T_D^{\mathrm{mix}} : H^{-\frac{1}{2}}(\partial D_1) \times H^{\frac{1}{2}}(\partial D_2) \to H^{\frac{1}{2}}(\partial D_1) \times H^{-\frac{1}{2}}(\partial D_2)$ *is of the form*

$$T_D^{\mathrm{mix}} \, = \, \left(\begin{bmatrix} S_{D_1} & 0 \\ 0 & N_{D_2} \end{bmatrix} + K_D^{\mathrm{mix}} \right),$$

and $K_D^{\mathrm{mix}} : H^{-\frac{1}{2}}(\partial D_1) \times H^{\frac{1}{2}}(\partial D_2) \to H^{\frac{1}{2}}(\partial D_1) \times H^{-\frac{1}{2}}(\partial D_2)$ *is compact.*

(b) G_D^{mix} *is compact and one-to-one with dense range in* $L^2(S^{d-1})$.

Proof. This is shown in [31, Thms. 3.2 and 3.4]. □

Finally, let $B \subseteq \mathbb{R}^d$ be open and Lipschitz bounded. We define the *Herglotz operators*

$$H_B : L^2(S^{d-1}) \to H^{\frac{1}{2}}(\partial B), \quad (H_B\phi)(x) := \int_{S^{d-1}} e^{ikx\cdot\theta}\phi(\theta)\,\mathrm{d}s(\theta), \tag{3.4}$$

and

$$\partial H_B : L^2(S^{d-1}) \to H^{-\frac{1}{2}}(\partial B), \quad (\partial H_B\phi)(x) := \frac{\partial}{\partial\nu(x)} \int_{S^{d-1}} e^{ikx\cdot\theta}\phi(\theta)\,\mathrm{d}s(\theta)\,.$$

From the asymptotic behavior of the fundamental solution Φ_k we obtain that $H_B^*\phi$, $\phi \in H^{-\frac{1}{2}}(\partial B)$, is just the far field pattern of the *single layer potential*

$$(\mathrm{SL}_B\phi)(x) := \int_{\partial B} \Phi_k(x,y)\phi(y)\,\mathrm{d}s(y), \qquad x \in \mathbb{R}^d \setminus \partial B\,.$$

We will use the relation

$$H_B^* \, = \, G_B^{\mathrm{dir}}S_B \qquad \text{or equivalently} \qquad H_B \, = \, S_B^*G_B^{\mathrm{dir}*} \tag{3.5}$$

(see [31, p. 18]).

4 Localized wave functions

In this section we establish the existence of *localized wave functions*. These are pairs of certain wave functions such that one component has arbitrarily large norm on some prescribed boundary while the other component has arbitrarily small norm on some different boundary. These localized wave functions will be essential in the proof of the monotonicity based shape characterization in Section 5 below.

4.1 Dirichlet or Neumann obstacles

To start with, we consider the case when either only Dirichlet or Neumann obstacles are present.

Let $B \subseteq \mathbb{R}^d$ be open and Lipschitz bounded, and let $\Gamma \subseteq \partial B$ be relatively open. We define the *restriction operator*

$$R_\Gamma : H^{\frac{1}{2}}(\partial B) \to H^{\frac{1}{2}}(\Gamma), \quad R_\Gamma f := f|_\Gamma,$$

and we note that the adjoint operator satisfies

$$R_\Gamma^* : \widetilde{H}^{-\frac{1}{2}}(\Gamma) \to H^{-\frac{1}{2}}(\partial B), \quad R_\Gamma^* f = \begin{cases} f & \text{on } \Gamma, \\ 0 & \text{on } \partial B \setminus \Gamma. \end{cases}$$

Here, $\widetilde{H}^{-\frac{1}{2}}(\Gamma)$ denotes the dual space of $H^{\frac{1}{2}}(\Gamma)$ (see, e.g., [33, p. 99]). Accordingly, we introduce

$$H_\Gamma := R_\Gamma H_B \qquad \text{and note that} \qquad H_\Gamma^* = H_B^* R_\Gamma^* = G_B^{\mathrm{dir}} S_B R_\Gamma^*. \tag{4.1}$$

Since (4.1) remains true if we modify ∂B away from Γ, we can w.l.o.g. assume that k^2 is not a Dirichlet eigenvalue of $-\Delta$ in B. Then S_B and G_B^{dir} are injective (cf. Theorem 3.2 (b)–(c)), and since $\mathcal{R}(R_\Gamma^*)$ has infinite dimensional range, this shows that $\mathcal{R}(H_\Gamma^*)$ is infinite dimensional as well.

Theorem 4.1 (Localized wave functions for Dirichlet obstacles). *Let $D_2 = \emptyset$, and let $B, D_1 \subseteq \mathbb{R}^d$ be open and Lipschitz bounded such that $\mathbb{R}^d \setminus \overline{D_1}$ is connected. Suppose that $B \not\subseteq D_1$. Then, for any finite dimensional subspace $V \subseteq L^2(S^{d-1})$ there exists a sequence $(\psi_m)_{m \in \mathbb{N}} \subseteq V^\perp$ such that*

$$\|H_B \psi_m\|_{H^{\frac{1}{2}}(\partial B)} \to \infty \qquad \text{and} \qquad \|G_{D_1}^{\mathrm{dir}\,*} \psi_m\|_{H^{-\frac{1}{2}}(\partial D_1)} \to 0 \qquad \text{as } m \to \infty.$$

The proof of Theorem 4.1 relies on the following lemmas.

Lemma 4.2. *Let $D_2 = \emptyset$, and let $B, D_1 \subseteq \mathbb{R}^d$ be open and Lipschitz bounded. Suppose that $B \not\subseteq D_1$, and let $\Gamma \subseteq \partial B \setminus \overline{D_1}$ be relatively open such that $\mathbb{R}^d \setminus (\overline{\Gamma \cup D_1})$ is connected. Then*

$$\mathcal{R}(H_\Gamma^*) \cap \mathcal{R}(G_{D_1}^{\mathrm{dir}}) = \{0\}.$$

Proof. Let $h \in \mathcal{R}(H_\Gamma^*) \cap \mathcal{R}(G_{D_1}^{\mathrm{dir}})$. Then there exist $f_\Gamma \in \widetilde{H}^{-\frac{1}{2}}(\Gamma)$ and $f_1 \in H^{\frac{1}{2}}(\partial D_1)$ such that

$$h = H_\Gamma^* f_\Gamma = G_{D_1}^{\mathrm{dir}} f_1.$$

Accordingly,

$$h = v_\Gamma^\infty = w_1^\infty,$$

7

where $v_\Gamma = \mathrm{SL}_B R_\Gamma^* f_\Gamma \in H^1_{\mathrm{loc}}(\mathbb{R}^d \setminus \overline{\Gamma})$ and $w_1 \in H^1_{\mathrm{loc}}(\mathbb{R}^d \setminus \overline{D_1})$ are radiating solutions to

$$\Delta v_\Gamma + k^2 v_\Gamma \;=\; 0 \quad \text{in } \mathbb{R}^d \setminus \overline{\Gamma} \qquad \text{and} \qquad \Delta w_1 + k^2 w_1 \;=\; 0 \quad \text{in } \mathbb{R}^d \setminus \overline{D_1}\,,$$

respectively. Rellich's lemma (cf., e.g., [9, Thm. 2.14]) and unique continuation guarantee that $v_\Gamma = w_1$ in $\mathbb{R}^d \setminus (\overline{\Gamma \cup D_1})$. We define $w \in H^1_{\mathrm{loc}}(\mathbb{R}^d)$ by

$$w \;:=\; \begin{cases} v_\Gamma = w_1 & \text{in } \mathbb{R}^d \setminus (\overline{\Gamma \cup D_1})\,, \\ w_1 & \text{on } \Gamma\,, \\ v_\Gamma & \text{in } D_1\,. \end{cases}$$

Then w is an entire radiating solution to the Helmholtz equation, and thus $w = 0$ in $\mathbb{R}^d$. This shows that $h = w_1^\infty = 0$. $\qquad\square$

In the next lemma we quote a special case of Lemma 2.5 in [14].

Lemma 4.3. *Let X, Y and Z be Hilbert spaces, and let $A : X \to Y$ and $B : X \to Z$ be bounded linear operators. Then,*

$$\exists C > 0 : \; \|Ax\| \le C \|Bx\| \quad \forall x \in X \qquad \text{if and only if} \qquad \mathcal{R}(A^*) \subseteq \mathcal{R}(B^*)\,.$$

Now we give the proof of Theorem 4.1.

Proof of Theorem 4.1. Let $D_2 = \emptyset$, and let $B, D_1 \subseteq \mathbb{R}^d$ be open and Lipschitz bounded such that $\mathbb{R}^d \setminus \overline{D_1}$ is connected, and suppose that $B \not\subseteq D_1$. Let $V \subseteq L^2(S^{d-1})$ be a finite dimensional subspace. We denote by $P_V : L^2(S^{d-1}) \to L^2(S^{d-1})$ the orthogonal projection onto V.

Since $B \not\subseteq D_1$, there exists $\Gamma \subseteq \partial B \setminus \overline{D_1}$ relatively open such that $\mathbb{R}^d \setminus (\overline{\Gamma \cup D_1})$ is connected. Applying Lemma 4.2 we find that

$$\mathcal{R}(H_\Gamma^*) \cap \mathcal{R}(G_{D_1}^{\mathrm{dir}}) \;=\; \{0\}\,,$$

and we have seen before that $\mathcal{R}(H_\Gamma^*)$ is infinite dimensional. Using a simple dimensionality argument (see [25, Lmm. 4.7]) it follows that

$$\mathcal{R}(H_\Gamma^*) \not\subseteq \mathcal{R}(G_{D_1}^{\mathrm{dir}}) + V \;=\; \mathcal{R}\big(\begin{bmatrix} G_{D_1}^{\mathrm{dir}} & P_V \end{bmatrix}\big)\,.$$

Accordingly, Lemma 4.3 implies that there is no constant $C > 0$ such that

$$\begin{aligned}
\|H_\Gamma \psi\|^2_{H^{\frac{1}{2}}(\Gamma)} &\le C^2 \left\| \begin{bmatrix} G_{D_1}^{\mathrm{dir}\,*} \\ P_V \end{bmatrix} \psi \right\|^2_{H^{-\frac{1}{2}}(\partial D_1) \times L^2(S^{d-1})} \\
&= C^2 \big(\|G_{D_1}^{\mathrm{dir}\,*} \psi\|^2_{H^{-\frac{1}{2}}(\partial D_1)} + \|P_V \psi\|^2_{L^2(S^{d-1})} \big)\,.
\end{aligned}$$

Thus, there exists a sequence $(\widetilde{\psi}_m)_{m \in \mathbb{N}} \subseteq L^2(S^{d-1})$ satisfying

$$\|H_\Gamma \widetilde{\psi}_m\|^2_{H^{\frac{1}{2}}(\Gamma)} \to \infty \qquad \text{and} \qquad \|G_{D_1}^{\mathrm{dir}\,*} \widetilde{\psi}_m\|^2_{H^{-\frac{1}{2}}(\partial D_1)} + \|P_V \widetilde{\psi}_m\|^2_{L^2(S^{d-1})} \to 0$$

8

as $m \to \infty$. We define $\psi_m := \widetilde{\psi}_m - P_V \widetilde{\psi}_m \subseteq V^\perp$ for any $m \in \mathbb{N}$ to obtain

$$\|H_\Gamma \psi_m\|_{H^{\frac{1}{2}}(\Gamma)} \;\geq\; \|H_\Gamma \widetilde{\psi}_m\|_{H^{\frac{1}{2}}(\Gamma)} - \|H_\Gamma\|\|P_V \widetilde{\psi}_m\|_{L^2(S^{d-1})} \to \infty\,,$$

$$\|G_{D_1}^{\mathrm{dir}\,*} \psi_m\|_{H^{-\frac{1}{2}}(\partial D_1)} \;\leq\; \|G_{D_1}^{\mathrm{dir}\,*} \widetilde{\psi}_m\|_{H^{-\frac{1}{2}}(\partial D_1)} + \|G_{D_1}^{\mathrm{dir}\,*}\|\|P_V \widetilde{\psi}_m\|_{L^2(S^{d-1})} \to 0$$

as $m \to \infty$. Recalling (4.1) we find that

$$\|R_\Gamma\|\|H_B \psi_m\|_{H^{\frac{1}{2}}(\partial B)} \;\geq\; \|H_\Gamma \psi_m\|_{H^{\frac{1}{2}}(\Gamma)}\,,$$

which ends the proof. $\qquad\square$

Using similar arguments the following result for Neumann obstacles can be shown.

Theorem 4.4 (Localized wave functions for Neumann obstacles). *Let $D_1 = \emptyset$, and let $B, D_2 \subseteq \mathbb{R}^d$ be open and Lipschitz bounded such that $\mathbb{R}^d \setminus \overline{D_2}$ is connected. Suppose that $B \not\subseteq D_2$. Then, for any finite dimensional subspace $V \subseteq L^2(S^{d-1})$ there exists a sequence $(\psi_m)_{m \in \mathbb{N}} \subseteq V^\perp$ such that*

$$\|H_B \psi_m\|_{H^{\frac{1}{2}}(\partial B)} \to \infty \qquad \text{and} \qquad \|G_{D_2}^{\mathrm{neu}*} \psi_m\|_{H^{\frac{1}{2}}(\partial D_2)} \to 0 \qquad \text{as } m \to \infty\,.$$

4.2   Mixed obstacles

For the general mixed case, i.e., when both Dirichlet and Neumann obstacles are present, we require a refined version of the Theorems 4.1 and 4.4, which we call *simultaneously localized wave functions* (see also [21], where a similar construction has been used).

To begin with, we define additional *restriction operators*. Let

$$R_{D_1} : H^{-\frac{1}{2}}(\partial D_1) \times H^{\frac{1}{2}}(\partial D_2) \to H^{-\frac{1}{2}}(\partial D_1)\,, \quad R_{D_1}(f,g) := f\,, \tag{4.2a}$$

$$R_{D_2} : H^{-\frac{1}{2}}(\partial D_1) \times H^{\frac{1}{2}}(\partial D_2) \to H^{\frac{1}{2}}(\partial D_2)\,, \quad R_{D_2}(f,g) := g\,. \tag{4.2b}$$

Then the adjoint operators satisfy

$$R_{D_1}^* : H^{\frac{1}{2}}(\partial D_1) \to H^{\frac{1}{2}}(\partial D_1) \times H^{-\frac{1}{2}}(\partial D_2)\,, \quad R_{D_1}^* f = (f, 0)\,,$$

$$R_{D_2}^* : H^{-\frac{1}{2}}(\partial D_2) \to H^{\frac{1}{2}}(\partial D_1) \times H^{-\frac{1}{2}}(\partial D_2)\,, \quad R_{D_2}^* g = (0, g)\,.$$

Furthermore, given an open and Lipschitz bounded $D_1 \subseteq \mathbb{R}^d$ and $\Gamma \subseteq \partial D_1$ relatively open we define

$$\widetilde{R_\Gamma} : H^{-\frac{1}{2}}(\partial D_1) \to H^{-\frac{1}{2}}(\Gamma)\,, \quad \widetilde{R_\Gamma} f := f|_\Gamma\,.$$

We note that the adjoint operator satisfies

$$\widetilde{R_\Gamma}^* : \widetilde{H}^{\frac{1}{2}}(\Gamma) \to H^{\frac{1}{2}}(\partial D_1)\,, \quad \widetilde{R_\Gamma}^* f = \begin{cases} f & \text{on } \Gamma\,, \\ 0 & \text{on } \partial D_1 \setminus \Gamma\,. \end{cases}$$

Here, $\widetilde{H}^{\frac{1}{2}}(\Gamma)$ denotes the dual space of $H^{-\frac{1}{2}}(\Gamma)$ (see, e.g., [33, p. 99]).

Theorem 4.5. *Let $B, D_1, D_2 \subseteq \mathbb{R}^d$ be open and Lipschitz bounded such that $\mathbb{R}^d \setminus (\overline{B \cup D_1 \cup D_2})$ is connected. Suppose that ∂D_1 is piecewise C^1 smooth and that $D_1 \not\subseteq B$. Then, for any finite dimensional subspace $V \subseteq L^2(S^{d-1})$ there exists a sequence $(\psi_m)_{m \in \mathbb{N}} \subseteq V^\perp$ such that*

$$\|(R_{D_1} G_D^{\mathrm{mix}*})\psi_m\|_{H^{-\frac{1}{2}}(\partial D_1)} \to \infty \quad and \quad \|(R_{D_2} G_D^{\mathrm{mix}*})\psi_m\|_{H^{\frac{1}{2}}(\partial D_2)} + \|H_B \psi_m\|_{H^{\frac{1}{2}}(\partial B)} \to 0$$

as $m \to \infty$.

The proof of Theorem 4.5 relies on the following lemma.

Lemma 4.6. *Let $B, D_1, D_2 \subseteq \mathbb{R}^d$ be open and Lipschitz bounded. Suppose that $D_1 \not\subseteq B$ and $\mathbb{R}^d \setminus (\overline{B \cup D_1 \cup D_2})$ is connected. Let $\Gamma \subseteq \partial D_1 \setminus \overline{B}$ be relatively open and C^1 smooth. Then*

$$\mathcal{R}(G_D^{\mathrm{mix}} R_{D_1}^* \widetilde{R_\Gamma}^*) \not\subseteq \mathcal{R}([G_D^{\mathrm{mix}} R_{D_2}^* \quad H_B^*])$$

and there exists an infinite dimensional subspace $Z \subseteq \mathcal{R}(G_D^{\mathrm{mix}} R_{D_1}^* \widetilde{R_\Gamma}^*)$ such that

$$Z \cap \mathcal{R}([G_D^{\mathrm{mix}} R_{D_2}^* \quad H_B^*]) = \{0\}.$$

Proof. Let $h \in \mathcal{R}(G_D^{\mathrm{mix}} R_{D_1}^* \widetilde{R_\Gamma}^*) \cap \mathcal{R}([G_D^{\mathrm{mix}} R_{D_2}^* \quad H_B^*])$. Then there are $f_\Gamma \in \widetilde{H}^{\frac{1}{2}}(\Gamma)$, $f_2 \in H^{-\frac{1}{2}}(\partial D_2)$ and $f_B \in H^{-\frac{1}{2}}(\partial B)$ such that

$$h = (G_D^{\mathrm{mix}} R_{D_1}^* \widetilde{R_\Gamma}^*) f_\Gamma = (G_D^{\mathrm{mix}} R_{D_2}^*) f_2 + H_B^* f_B.$$

Accordingly,

$$h = w_1^\infty = w_2^\infty + v_B^\infty,$$

where $w_1, w_2 \in H^1_{\mathrm{loc}}(\mathbb{R}^d \setminus (\overline{D_1 \cup D_2}))$ and $v_B = \mathrm{SL}_B f_B \in H^1_{\mathrm{loc}}(\mathbb{R}^d \setminus \overline{\partial B})$ are radiating solutions to

$$\Delta w_1 + k^2 w_1 = 0 \quad \text{in } \mathbb{R}^d \setminus (\overline{D_1 \cup D_2}), \quad w_1 = \widetilde{R_\Gamma}^* f_\Gamma \quad \text{on } \partial D_1, \quad \frac{\partial w_1}{\partial \nu} = 0 \quad \text{on } \partial D_2,$$

$$\Delta w_2 + k^2 w_2 = 0 \quad \text{in } \mathbb{R}^d \setminus (\overline{D_1 \cup D_2}), \quad w_2 = 0 \quad \text{on } \partial D_1, \quad \frac{\partial w_2}{\partial \nu} = f_2 \quad \text{on } \partial D_2,$$

$$\Delta v_B + k^2 v_B = 0 \quad \text{in } \mathbb{R}^d \setminus \overline{\partial B}.$$

Rellich's lemma and unique continuation guarantee that $w_1 = w_2 + v_B$ in $\mathbb{R}^d \setminus (\overline{B \cup D_1 \cup D_2})$. Therefore,

$$f_\Gamma = w_1|_\Gamma = v_B|_\Gamma = (\mathrm{SL}_B f_B)|_\Gamma.$$

Since Γ is C^1 smooth,[2] this and the smoothness of $\mathrm{SL}_B f_B$ away from ∂B imply that $f_\Gamma \in C^1(\Gamma)$. Without loss of generality we assume that

$$\Gamma = \{x \in \mathbb{R}^d \mid x_d = \zeta(x') \text{ for all } x' = (x_1, \ldots, x_{d-1}) \in B'_r(0)\}$$

for some C^1 function $\zeta : \mathbb{R}^{d-1} \to \mathbb{R}$, where $B'_r(0) \subseteq \mathbb{R}^{d-1}$ denotes the $d - 1$ dimensional ball of radius $r > 0$ around zero. We call $u \in H^{\frac{1}{2}}(\Gamma)$ piecewise linear on Γ, if the function u_ζ given by

$$u_\zeta(x') := u(x', \zeta(x')), \qquad x' \in B'_r(0),$$

---

[2]This is the only argument where we utilize the additional smoothness of $\Gamma \subseteq \partial D_1$.

is piecewise linear on $B'_r(0) \subseteq \mathbb{R}^{d-1}$. Denoting by $X \subseteq H^{\frac{1}{2}}(\Gamma)$ the subspace of piecewise linear continuous functions on Γ that vanish on $\partial\Gamma$,[3] we obtain that $Z := G_D^{\mathrm{mix}} R_{D_1}^* \widetilde{R_\Gamma}^*(X)$ satisfies

$$Z \cap \mathcal{R}\left(\begin{bmatrix} G_D^{\mathrm{mix}} R_{D_2}^* & H_B^* \end{bmatrix}\right) = \{0\}.$$

Since X is infinite dimensional and $G_D^{\mathrm{mix}} R_{D_1}^* \widetilde{R_\Gamma}^*$ is one-to-one (see Theorem 3.6 (b)), we find that Z is infinite dimensional as well. □

Now we give the proof of Theorem 4.5.

Proof of Theorem 4.5. Let $B, D_1, D_2 \subseteq \mathbb{R}^d$ be open and Lipschitz bounded such that the complement $\mathbb{R}^d \setminus (\overline{B \cup D_1 \cup D_2})$ is connected. Suppose that ∂D_1 is piecewise C^1 smooth and that $D_1 \not\subseteq B$. Let $V \subseteq L^2(S^{d-1})$ be a finite dimensional subspace. We denote by $P_V : L^2(S^{d-1}) \to L^2(S^{d-1})$ the orthogonal projection onto V.

Since $D_1 \not\subseteq B$ and ∂D_1 is piecewise C^1 smooth, there exists $\Gamma \subseteq \partial D_1 \setminus \overline{B}$ relatively open such that Γ is C^1 smooth. Combining Lemma 4.6 with a simple dimensionality argument (see [25, Lmm. 4.7]) we find that

$$Z \not\subseteq \mathcal{R}(\begin{bmatrix} G_D^{\mathrm{mix}} R_{D_2}^* & H_B^* \end{bmatrix}) + V = \mathcal{R}(\begin{bmatrix} G_D^{\mathrm{mix}} R_{D_2}^* & H_B^* & P_V \end{bmatrix}).$$

where $Z \subseteq \mathcal{R}(G_D^{\mathrm{mix}} R_{D_1}^* \widetilde{R_\Gamma}^*)$ denotes the subspace in Lemma 4.6, and thus

$$\mathcal{R}(G_D^{\mathrm{mix}} R_{D_1}^* \widetilde{R_\Gamma}^*) \not\subseteq \mathcal{R}(\begin{bmatrix} G_D^{\mathrm{mix}} R_{D_2}^* & H_B^* \end{bmatrix}) + V = \mathcal{R}(\begin{bmatrix} G_D^{\mathrm{mix}} R_{D_2}^* & H_B^* & P_V \end{bmatrix}).$$

Accordingly, Lemma 4.3 implies that there is no constant $C > 0$ such that

$$\|(\widetilde{R_\Gamma} R_{D_1} G_D^{\mathrm{mix}*})\psi\|^2_{H^{-\frac{1}{2}}(\Gamma)} \leq C^2 \left\| \begin{bmatrix} R_{D_2} G_D^{\mathrm{mix}*} \\ H_B \\ P_V \end{bmatrix} \psi \right\|^2_{H^{\frac{1}{2}}(\partial D_2) \times H^{\frac{1}{2}}(\partial B) \times L^2(S^{d-1})}$$

$$= C^2 \left(\|(R_{D_2} G_D^{\mathrm{mix}*})\psi\|^2_{H^{\frac{1}{2}}(\partial D_2)} + \|H_B\psi\|^2_{H^{\frac{1}{2}}(\partial B)} + \|P_V\psi\|^2_{L^2(S^{d-1})} \right).$$

Therefore, there exists a sequence $(\widetilde{\psi}_m)_{m \in \mathbb{N}} \subseteq L^2(S^{d-1})$ satisfying

$$\|(\widetilde{R_\Gamma} R_{D_1} G_D^{\mathrm{mix}*})\widetilde{\psi}_m\|^2_{H^{-\frac{1}{2}}(\Gamma)} \to \infty$$

and

$$\|(R_{D_2} G_D^{\mathrm{mix}*})\widetilde{\psi}_m\|^2_{H^{\frac{1}{2}}(\partial D_2)} + \|H_B\widetilde{\psi}_m\|^2_{H^{\frac{1}{2}}(\partial B)} + \|P_V\widetilde{\psi}_m\|^2_{L^2(S^{d-1})} \to 0$$

as $m \to \infty$. We define $\psi_m := \widetilde{\psi}_m - P_V\widetilde{\psi}_m \subseteq V^\perp$ for any $m \in \mathbb{N}$ to obtain

$$\|(R_{D_1} G_D^{\mathrm{mix}*})\psi_m\|_{H^{-\frac{1}{2}}(\partial D_1)} \geq \|(\widetilde{R_\Gamma} R_{D_1} G_D^{\mathrm{mix}*})\psi_m\|_{H^{-\frac{1}{2}}(\Gamma)}$$

$$\geq \|(\widetilde{R_\Gamma} R_{D_1} G_D^{\mathrm{mix}*})\widetilde{\psi}_m\|_{H^{-\frac{1}{2}}(\Gamma)} - \|\widetilde{R_\Gamma} R_{D_1} G_D^{\mathrm{mix}*}\|\|P_V\widetilde{\psi}_m\|_{L^2(S^{d-1})} \to \infty,$$

$$\|(R_{D_2} G_D^{\mathrm{mix}*})\psi_m\|_{H^{\frac{1}{2}}(\partial D_2)} \leq \|(R_{D_2} G_D^{\mathrm{mix}*})\widetilde{\psi}_m\|_{H^{\frac{1}{2}}(\partial D_2)} + \|R_{D_2} G_D^{\mathrm{mix}*}\|\|P_V\widetilde{\psi}_m\|_{L^2(S^{d-1})} \to 0,$$

$$\|H_B\psi_m\|_{H^{\frac{1}{2}}(\partial B)} \leq \|H_B\widetilde{\psi}_m\|_{H^{\frac{1}{2}}(\partial B)} + \|H_B\|\|P_V\widetilde{\psi}_m\|_{L^2(S^{d-1})} \to 0$$

as $m \to \infty$. This ends the proof. □

---

[3]The latter condition ensures that X does not contain any smooth functions except for zero.

The following result can be shown proceeding similarly to the proof of Theorem 4.5.

Theorem 4.7. *Let $B, D_1, D_2 \subseteq \mathbb{R}^d$ be open and Lipschitz bounded such that $\mathbb{R}^d \setminus (\overline{B \cup D_1 \cup D_2})$ is connected. Suppose that ∂D_2 is piecewise C^1 smooth and that $D_2 \not\subseteq B$. Then, for any finite dimensional subspace $V \subseteq L^2(S^{d-1})$ there exists a sequence $(\psi_m)_{m \in \mathbb{N}} \subseteq V^\perp$ such that*

$$\|(R_{D_1} G_D^{\mathrm{mix}*})\psi_m\|_{H^{-\frac{1}{2}}(\partial D_1)} + \|H_B \psi_m\|_{H^{\frac{1}{2}}(\partial B)} \to 0 \quad and \quad \|(R_{D_2} G_D^{\mathrm{mix}*})\psi_m\|_{H^{\frac{1}{2}}(\partial D_2)} \to \infty$$

as $m \to \infty$.

5   Monotonicity based shape reconstruction

Using the localized wave functions developed in the previous section will establish monotonicity relations for far field operators in terms of the following extension of the Loewner order to compact self-adjoint operators, which has been introduced in [25]. Let $A_1, A_2 : X \to X$ be compact self-adjoint operators on a Hilbert space X, and let $r \in \mathbb{N}$. We write

$$A_1 \leq_r A_2$$

if $A_2 - A_1$ has at most r negative eigenvalues. Furthermore, we write $A_1 \leq_{\mathrm{fin}} A_2$ if $A_1 \leq_r A_2$ holds for some $r \in \mathbb{N}$.

Remark 5.1. Therewith, Remarks 3.3 and 3.5 can be reformulated as

$$\mathrm{Re}(F_{D_1}^{\mathrm{dir}}) \leq_{\mathrm{fin}} 0 \qquad and \qquad \mathrm{Re}(F_{D_2}^{\mathrm{neu}}) \geq_{\mathrm{fin}} 0\,,$$

respectively. $\Diamond$

The following result was shown in [25, Cor. 3.3].

Lemma 5.2. *Let $A_1, A_2 : X \to X$ be two compact self-adjoint linear operators on a Hilbert space X with scalar product $\langle \cdot, \cdot \rangle$, and let $r \in \mathbb{N}$. Then the following statements are equivalent:*

(a) $A_1 \leq_r A_2$

(b) *There exists a finite-dimensional subspace $V \subseteq X$ with $\dim(V) \leq r$ such that*

$$\langle (A_2 - A_1)v, v \rangle \geq 0 \qquad for\ all\ v \in V^\perp\,.$$

5.1   Dirichlet or Neumann obstacles

In the following we consider the case when either only Dirichlet or Neumann obstacles are present. We discuss criteria to characterize the support of an unknown scattering obstacle D in terms of the corresponding far field operator. To begin with, we discuss the case when only Dirichlet obstacles are present.

Theorem 5.3 (Shape characterization for Dirichlet obstacles)**.** *Let $D_2 = \emptyset$, and let $B, D_1 \subseteq \mathbb{R}^d$ be open and Lipschitz bounded such that $\mathbb{R}^d \setminus \overline{D_1}$ is connected.*

(a) *If $\overline{B} \subseteq D_1$, then $\mathrm{Re}(F_{D_1}^{\mathrm{dir}}) \leq_{\mathrm{fin}} -H_B^* H_B$.*

12

(b) If $B \not\subseteq D_1$, then $\mathrm{Re}(F_{D_1}^{\mathrm{dir}}) \not\preceq_{\mathrm{fin}} -H_B^* H_B$.

Proof. (a) Let $\overline{B} \subseteq D_1$. We define $P_{B \to D_1}^{\mathrm{dir}} : H^{\frac{1}{2}}(\partial B) \to H^{\frac{1}{2}}(\partial D_1)$ by $P_{B \to D_1}^{\mathrm{dir}} f := w|_{\partial D_1}$, where $w \in H_{\mathrm{loc}}^1(\mathbb{R}^d \setminus \overline{B})$ is the unique radiating solution to the exterior Dirichlet boundary value problem (2.3a)–(2.3b) with D_1 replaced by B (and $D_2 = \emptyset$). Then P^{dir} is a compact linear operator by standard interior regularity results, and the uniqueness of solutions to the exterior Dirichlet boundary value problem (see Lemma 2.1) implies that $G_B^{\mathrm{dir}} = G_{D_1}^{\mathrm{dir}} P_{B \to D_1}^{\mathrm{dir}}$. Recalling (3.5), this shows that

$$H_B = S_B^* (P_{B \to D_1}^{\mathrm{dir}})^* G_{D_1}^{\mathrm{dir}\,*}.$$

Substituting the factorization (3.3) gives

$$\mathrm{Re}(F_{D_1}^{\mathrm{dir}}) + H_B^* H_B = -G_{D_1}^{\mathrm{dir}} \Big(\frac{1}{2}(S_{D_1} + S_{D_1}^*) - P_{B \to D_1}^{\mathrm{dir}} S_B S_B^* (P_{B \to D_1}^{\mathrm{dir}})^* \Big) G_{D_1}^{\mathrm{dir}\,*}.$$

Using Theorem 3.2 (d)–(e) we find that $\frac{1}{2}(S_{D_1} + S_{D_1}^*)$ is a compact perturbation of the self-adjoint and coercive operator $S_{D_1,\mathrm{i}}$, i.e.,

$$\mathrm{Re}(F_{D_1}^{\mathrm{dir}}) + H_B^* H_B = -G_{D_1}^{\mathrm{dir}} \big(S_{D_1,\mathrm{i}} + K \big) G_{D_1}^{\mathrm{dir}\,*}$$

with some compact self-adjoint operator K. Accordingly,

$$\langle (\mathrm{Re}(F_{D_1}^{\mathrm{dir}}) + H_B^* H_B)\psi, \psi \rangle \leq -c_1 \|G_{D_1}^{\mathrm{dir}\,*}\psi\|_{H^{-1/2}(\partial D_1)}^2 + \langle G_{D_1}^{\mathrm{dir}\,*}\psi, K G_{D_1}^{\mathrm{dir}\,*}\psi \rangle$$

for all $\psi \in L^2(S^{d-1})$, where c_1 denotes the coercivity constant of $S_{D_1,\mathrm{i}}$ (see Theorem 3.2 (d)). We define the subspace

$$V := \mathrm{span}\Big\{ \psi \in L^2(S^{d-1}) \ \Big| \ G_{D_1}^{\mathrm{dir}\,*}\psi \text{ is an eigenvector of } K$$

$$\text{associated to an eigenvalue larger than } c_1 \Big\}.$$

The spectral theorem for compact self-adjoint operators shows that V is finite dimensional. Accordingly,

$$\langle (\mathrm{Re}(F_{D_1}^{\mathrm{dir}}) + H_B^* H_B)\psi, \psi \rangle \leq 0 \qquad \text{for all } \psi \in V^\perp.$$

(b) Let $B \not\subseteq D_1$. We suppose that there exists a finite dimensional subspace $V \subseteq L^2(S^{d-1})$ such that

$$\langle \mathrm{Re}(F_{D_1}^{\mathrm{dir}})\psi, \psi \rangle \leq -\langle H_B^* H_B \psi, \psi \rangle \qquad \text{for all } \psi \in V^\perp. \tag{5.1}$$

Again, using the factorization (3.3) we find that, for all $\psi \subseteq V^\perp$,

$$|\langle \mathrm{Re}(F_{D_1}^{\mathrm{dir}})\psi, \psi \rangle| \leq \|S_{D_1} + S_{D_1}^*\| \|G_{D_1}^{\mathrm{dir}\,*}\psi\|_{H^{-\frac{1}{2}}(\partial D_1)}^2 \leq C \|G_{D_1}^{\mathrm{dir}\,*}\psi\|_{H^{-\frac{1}{2}}(\partial D_1)}^2$$

for some $C > 0$, and on the other hand

$$\langle H_B^* H_B \psi, \psi \rangle = \|H_B \psi\|_{H^{\frac{1}{2}}(\partial B)}^2.$$

Substituting this into (5.1) and applying Theorem 4.1 gives a contradiction. $\square$

The following result for Neumann obstacles can be shown using similar arguments as in the proof of Theorem 5.3.

Theorem 5.4 (Shape characterization for Neumann obstacles)**.** *Let $D_1 = \emptyset$, and let $B, D_2 \subseteq \mathbb{R}^d$ be open and Lipschitz bounded such that $\mathbb{R}^d \setminus \overline{D_2}$ is connected.*

(a) *If $\overline{B} \subseteq D_2$, then $H_B^* H_B \leq_{\mathrm{fin}} \mathrm{Re}(F_{D_2}^{\mathrm{neu}})$.*

(b) *If $B \not\subseteq D_2$, then $H_B^* H_B \not\leq_{\mathrm{fin}} \mathrm{Re}(F_{D_2}^{\mathrm{neu}})$.*

5.2 Mixed obstacles

Next we consider the general mixed case, i.e., when both Dirichlet and Neumann obstacles are present. While the criteria developed in Theorems 5.3 and 5.4 determine whether a certain probing domain B is contained in the support D of the scattering obstacles or not, the criterion for the mixed case established in Theorem 5.5 below characterizes whether a certain probing domain B contains the support D of the scattering obstacles or not.

Theorem 5.5 (Shape characterization for mixed obstacles)**.** *Let $B, D_1, D_2 \subseteq \mathbb{R}^d$ be open and Lipschitz bounded. Assume that k^2 is neither a Dirichlet eigenvalue of $-\Delta$ in D_1 and B nor a Neumann eigenvalue of $-\Delta$ in D_2.*

(a) *If $\overline{D_1} \subseteq B$, then $-H_B^* H_B \leq_{\mathrm{fin}} \mathrm{Re}(F_D^{\mathrm{mix}})$.*

(b) *Suppose that $\mathbb{R}^d \setminus (\overline{B \cup D_1 \cup D_2})$ is connected and that ∂D_1 is piecewise C^1 smooth. If $D_1 \not\subseteq B$, then $-H_B^* H_B \not\leq_{\mathrm{fin}} \mathrm{Re}(F_D^{\mathrm{mix}})$.*

(c) *If $\overline{D_2} \subseteq B$, then $\mathrm{Re}(F_D^{\mathrm{mix}}) \leq_{\mathrm{fin}} H_B^* H_B$.*

(d) *Suppose that $\mathbb{R}^d \setminus (\overline{B \cup D_1 \cup D_2})$ is connected and that ∂D_2 is piecewise C^1 smooth. If $D_2 \not\subseteq B$, then $\mathrm{Re}(F_D^{\mathrm{mix}}) \not\leq_{\mathrm{fin}} H_B^* H_B$.*

Remark 5.6. The results in Theorem 5.5 remain true in the special case, when $D_2 = \emptyset$ and $F_D^{\mathrm{mix}} = F_{D_1}^{\mathrm{dir}}$, and also in the special case, when $D_1 = \emptyset$ and $F_D^{\mathrm{mix}} = F_{D_2}^{\mathrm{neu}}$. The corresponding shape characterizations complement the results established in Theorems 5.3 and 5.4. ◇

Proof. (a) Let $\overline{D_1} \subseteq B$. It has been shown in [31, Lmm. 3.5] that

$$\mathrm{Re}(F_D^{\mathrm{mix}}) + H_B^* H_B = \begin{bmatrix} H_B \\ (\partial H)_{D_2} \end{bmatrix}^* \left(\begin{bmatrix} I_{D_1} & 0 \\ 0 & -N_{D_2,\mathrm{i}}^{-1} \end{bmatrix} + K \right) \begin{bmatrix} H_B \\ (\partial H)_{D_2} \end{bmatrix}$$

with some compact self-adjoint operator K, i.e., $\mathrm{Re}(F_D^{\mathrm{mix}}) + H_B^* H_B$ is a compact perturbation of a self-adjoint and coercive operator. This implies (a).

(b) Let $\mathbb{R}^d \setminus (\overline{B \cup D_1 \cup D_2})$ be connected and let ∂D_1 be piecewise C^1 smooth. We suppose that there exists a finite dimensional subspace $V_1 \subseteq L^2(S^{d-1})$ such that

$$-\langle H_B^* H_B \psi, \psi \rangle \leq \langle \mathrm{Re}(F_D^{\mathrm{mix}}) \psi, \psi \rangle \qquad \text{for all } \psi \in V_1^{\perp}.$$

Combining Theorem 3.6 (a) with Theorems 3.2–3.4 (d)–(e), we find that

$$\mathrm{Re}(F_D^{\mathrm{mix}}) = \frac{1}{2}(F_D^{\mathrm{mix}} + F_D^{\mathrm{mix}*}) = -G_D^{\mathrm{mix}} \left(\begin{bmatrix} S_{D_1,\mathrm{i}} & 0 \\ 0 & N_{D_2,\mathrm{i}} \end{bmatrix} + K \right) G_D^{\mathrm{mix}*}$$

14

with some compact self-adjoint operator K. Accordingly, we define the subspace

$$V_2 := \operatorname{span}\Big\{ \psi \in L^2(S^{d-1}) \mid G_D^{\mathrm{mix}*}\psi \text{ is an eigenvector of } K$$

$$\text{associated to an eigenvalue with absolute value larger than } \frac{c_1}{2}\Big\},$$

where c_1 denotes the coercivity constant of $S_{D_1,\mathrm{i}}$ (see Theorem 3.2 (d)). The spectral theorem for compact self-adjoint operators shows that $V_2 \subseteq L^2(S^{d-1})$ is finite dimensional, and thus $V_1^\perp \cap V_2^\perp = (V_1 + V_2)^\perp \neq \{0\}$ because $V_1 + V_2$ is finite dimensional as well. Using the restriction operators R_{D_1} and R_{D_2} from (4.2), we find that, for all $\psi \in (V_1 + V_2)^\perp$,

$$
\begin{aligned}
0 &\leq \langle \operatorname{Re}(F_D^{\mathrm{mix}})\psi, \psi \rangle + \langle H_B^* H_B \psi, \psi \rangle \\
&= -\langle (G_D^{\mathrm{mix}} R_{D_1}^*) S_{D_1,\mathrm{i}} (G_D^{\mathrm{mix}} R_{D_1}^*)^* \psi, \psi \rangle - \langle (G_D^{\mathrm{mix}} R_{D_2}^*) N_{D_2,\mathrm{i}} (G_D^{\mathrm{mix}} R_{D_2}^*)^* \psi, \psi \rangle \\
&\quad - \langle G_D^{\mathrm{mix}} K G_D^{\mathrm{mix}*} \psi, \psi \rangle + \langle H_B^* H_B \psi, \psi \rangle \\
&\leq -c_1 \| (R_{D_1} G_D^{\mathrm{mix}*})\psi \|^2_{H^{-\frac{1}{2}}(\partial D_1)} + \|N_{D_2,\mathrm{i}}\| \| (R_{D_2} G_D^{\mathrm{mix}*})\psi \|^2_{H^{\frac{1}{2}}(\partial D_2)} \\
&\quad + \frac{c_1}{2} \| G_D^{\mathrm{mix}*}\psi \|^2_{H^{-\frac{1}{2}}(\partial D_1) \times H^{\frac{1}{2}}(\partial D_2)} + \|H_B\psi\|^2_{H^{\frac{1}{2}}(\partial B)} \\
&= -\frac{c_1}{2} \| (R_{D_1} G_D^{\mathrm{mix}*})\psi \|^2_{H^{-\frac{1}{2}}(\partial D_1)} + \Big(\|N_{D_2,\mathrm{i}}\| + \frac{c_1}{2} \Big) \| (R_{D_2} G_D^{\mathrm{mix}*})\psi \|^2_{H^{\frac{1}{2}}(\partial D_2)} + \|H_B\psi\|^2_{H^{\frac{1}{2}}(\partial B)}.
\end{aligned}
$$

Applying Theorem 4.5 with $V = V_1 + V_2$ gives a contradiction.

(c) This follows again from [31, Lmm. 3.5].

(d) This can be shown proceeding similarly to the proof of part (b), and using Theorem 4.7 to obtain a contradiction. $\qquad\square$

6 Numerical examples

We now work towards numerical implementations of the shape characterizations developed in Section 5. The main issue here is that numerical approximations of the operators $F_{D_1}^{\mathrm{dir}}$, $F_{D_2}^{\mathrm{neu}}$, F_D^{mix}, and H_B are necessarily finite dimensional. Accordingly, the question, whether suitable combinations of these operators as considered in Theorems 5.3–5.5 are positive definite up to some finite dimensional subspace, needs to be carefully relaxed to obtain reliable numerical algorithms. We present some preliminary ideas in this direction, restricting the discussion to the two-dimensional case.

6.1 An explicit radially symmetric example

We illustrate the shape characterization results from Theorems 5.3 and 5.5 for the special case of a single radially symmetric Dirichlet obstacle by an explicit example. Let $D_2 = \emptyset$, and let $D_1 = B_r(0) \subseteq \mathbb{R}^2$ be the disk of radius $r > 0$ centered at the origin.

We first derive series expansions for the incident and scattered fields and use them to compute the eigenvalue value decomposition of the far field operator $F_{D_1}^{\mathrm{dir}}$. The Jacobi-Anger expansion (see,

e.g., [9, (3.89)]) shows that for each incident direction $\theta = (\cos t, \sin t)^\top \in S^1$ the incident field satisfies

$$u^i(x;\theta) = e^{\mathrm{i}kx\cdot\theta} = \sum_{n\in\mathbb{Z}} \mathrm{i}^n e^{-\mathrm{i}n\phi_x} J_n(k|x|)e^{\mathrm{i}nt}, \qquad x = |x|(\cos\phi_x, \sin\phi_x)^\top \in \mathbb{R}^2.$$

A short calculation yields that the scattered field is given by

$$u^s(x;\theta) = -\sum_{n\in\mathbb{Z}} \mathrm{i}^n \frac{J_n(kr)}{H_n^{(1)}(kr)} e^{-\mathrm{i}n\phi_x} H_n^{(1)}(k|x|)e^{\mathrm{i}nt}, \qquad x = |x|(\cos\phi_x, \sin\phi_x)^\top \in \mathbb{R}^2 \setminus \overline{D_1}.$$

Substituting the asymptotic behavior of the Hankel functions (see, e.g., [9, (3.82)]) into this expansion we find that the far field pattern of u^s is

$$u^\infty(\widehat{x};\theta) = \sum_{n\in\mathbb{Z}} 4\mathrm{i} \frac{J_n(kr)}{H_n^{(1)}(kr)} e^{-\mathrm{i}n\phi_x} e^{\mathrm{i}nt}, \qquad \widehat{x} = (\cos\phi_x, \sin\phi_x)^\top \in S^1.$$

Let $g \in L^2(S^1)$ with Fourier expansion $g(\theta) = \sum_{m\in\mathbb{Z}} g_m e^{\mathrm{i}mt}$, $\theta = (\cos t, \sin t)^\top \in S^1$. Then the far field operator $F_{D_1}^{\mathrm{dir}} : L^2(S^1) \to L^2(S^1)$ from (2.5) satisfies

$$\begin{aligned}
(F_{D_1}^{\mathrm{dir}}g)(\widehat{x}) &= \sum_{n\in\mathbb{Z}}\sum_{m\in\mathbb{Z}} 4\mathrm{i} \frac{J_n(kr)}{H_n^{(1)}(kr)} \left(\int_0^{2\pi} g_m e^{\mathrm{i}(n+m)t}\,\mathrm{d}t\right) e^{-\mathrm{i}n\phi_x} \\
&= \sum_{n\in\mathbb{Z}} 8\pi\mathrm{i} \frac{J_n(kr)}{H_n^{(1)}(kr)} g_n e^{\mathrm{i}n\phi_x},
\end{aligned}$$

$\widehat{x} = (\cos\phi_x, \sin\phi_x)^\top \in S^1$. Accordingly, the eigenvalues and eigenvectors of $F_{D_1}^{\mathrm{dir}}$ are given by $(\lambda_n^{(r)}, v_n)_{n\in\mathbb{Z}}$ with

$$\lambda_n^{(r)} := 8\pi\mathrm{i} \frac{J_n(kr)}{H_n^{(1)}(kr)}, \qquad v_n(\widehat{x}) := \frac{1}{\sqrt{2\pi}} e^{\mathrm{i}n\phi_x}, \quad \widehat{x} = (\cos\phi_x, \sin\phi_x)^\top \in S^1. \qquad (6.1)$$

Now let $B = B_R(0)$ be the disk of radius $R > 0$ centered at the origin. Then the operator $H_B^* H_B : L^2(S^1) \to L^2(S^1)$, where H_B is the Herglotz operator from (3.4), satisfies

$$\begin{aligned}
(H_B^* H_B g)(\theta) &= \int_{S^1} \left(\int_{\partial B} e^{\mathrm{i}ky\cdot(\phi-\theta)}\,\mathrm{d}s(y)\right) g(\phi)\,\mathrm{d}s(\phi) \\
&= \int_{S^1} 2\pi R J_0(kR|\theta - \phi|)g(\phi)\,\mathrm{d}s(\phi).
\end{aligned} \qquad (6.2)$$

Here we used the integral representation of J_0 (see, e.g., [34, 10.9.2]). Writing $\phi = (\cos\tau, \sin\tau)$ and substituting the Fourier expansion of g we find that

$$(H_B^* H_B g)(\theta) = 2\pi R \sum_{n\in\mathbb{Z}} g_n \int_{S^1} J_0(kR|\theta - \phi|)e^{\mathrm{i}n\tau}\,\mathrm{d}s(\phi) = 4\pi^2 R \sum_{n\in\mathbb{Z}} g_n J_n^2(kR)e^{\mathrm{i}nt}$$

(see, e.g., [9, (3.88)]). Accordingly, the eigenvalues and eigenvectors of the operator $H_B^* H_B$ are given by $(\mu_n^{(R)}, v_n)_{n\in\mathbb{Z}}$ with

$$\mu_n^{(R)} := 4\pi^2 R J_n^2(kR), \qquad v_n(\widehat{x}) = \frac{1}{\sqrt{2\pi}} e^{\mathrm{i}n\phi_x}, \quad \widehat{x} = (\cos\phi_x, \sin\phi_x)^\top \in S^1. \qquad (6.3)$$
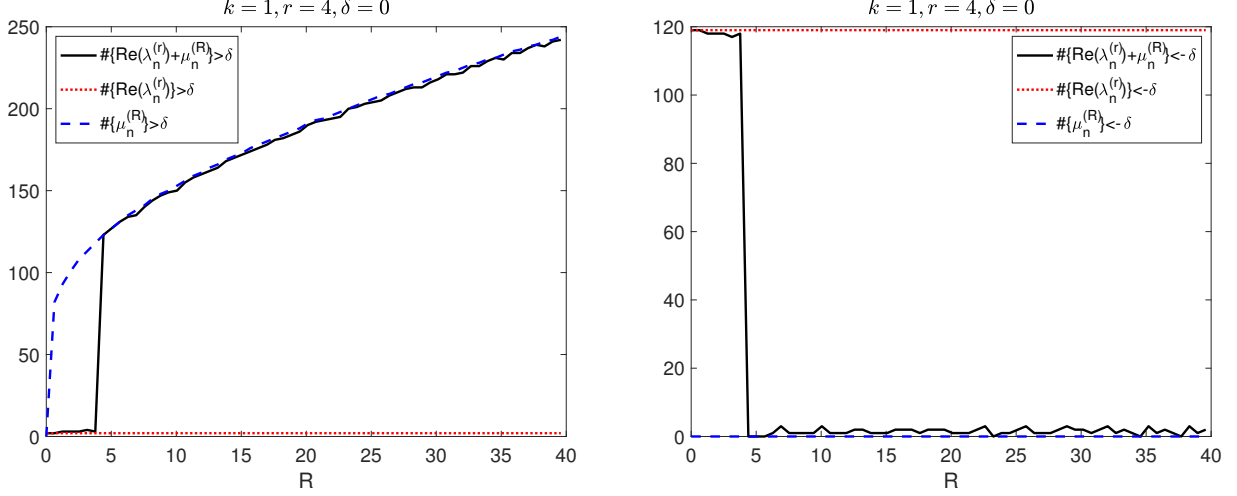
16

Figure 6.1: Number of positive eigenvalues (left) and number of negative eigenvalues (right) $\mathrm{Re}(\lambda_n^{(r)})$ (dotted), $\mu_n^{(R)}$ (dashed), and $\mathrm{Re}(\lambda_n^{(r)}) + \mu_n^{(R)}$ (solid) within range $n = 0, \ldots, 1000$ as function of R.

From (6.1) and (6.3) we conclude that in the special case, when $D_1 = B_r(0)$ and $B = B_R(0)$, the eigenvalues and eigenvectors of $\mathrm{Re}(F_{D_1}^{\mathrm{dir}}) + H_B^* H_B$ are given by $(\mathrm{Re}(\lambda_n^{(r)}) + \mu_n^{(R)}, v_n)_{n \in \mathbb{Z}}$ with

$$
\begin{aligned}
\mathrm{Re}(\lambda_n^{(r)}) + \mu_n^{(R)} &= 8\pi \frac{J_n(kr) Y_n(kr)}{|H_n^{(1)}(kr)|^2} + 4\pi^2 R J_n^2(kR)\,, \\
v_n(\widehat{x}) &= \frac{1}{\sqrt{2\pi}} e^{\mathrm{i} n \phi_x}\,, \qquad \widehat{x} = (\cos \phi_x, \sin \phi_x)^\top \in S^1\,.
\end{aligned}
\tag{6.4}
$$

Using the criteria established in Theorem 5.3 and Theorem 5.5 (a)–(b) we obtain that

(a) if $R < r$, then $\mathrm{Re}(F_{D_1}^{\mathrm{dir}}) + H_B^* H_B$ has only finitely many positive but infinitely many negative eigenvalues, and

(b) if $R > r$, then $\mathrm{Re}(F_{D_1}^{\mathrm{dir}}) + H_B^* H_B$ has only finitely many negative but infinitely many positive eigenvalues.

We illustrate how this can be utilized to reconstruct the radius of the scatterer $D_1 = B_r(0)$ from observations of $F_{D_1}^{\mathrm{dir}}$ by a numerical example. We evaluate the eigenvalues $\mathrm{Re}(\lambda_n^{(r)})$, $\mu_n^{(R)}$, and $\mathrm{Re}(\lambda_n^{(r)}) + \mu_n^{(R)}$ with wave number $k = 1$, radius of the obstacle $r = 4$, and $n = 0, \ldots, 1000$ in Matlab using the explicit formulas given in (6.1), (6.3), and (6.4). In Figure 6.1 we show plots of the number of positive eigenvalues (left plot) and of the number of negative eigenvalues (right plot) $\mathrm{Re}(\lambda_n^{(r)})$ (dotted), $\mu_n^{(R)}$ (dashed), and $\mathrm{Re}(\lambda_n^{(r)}) + \mu_n^{(R)}$ (solid) within the range $n = 0, \ldots, 1000$ as a function of R.

As suggested by Theorems 5.3 and 5.5 there is a sharp transition in the behavior of the eigenvalues of $\mathrm{Re}(F_{D_1}^{\mathrm{dir}}) + H_B^* H_B$ at $R = r = 4$, which can be used to estimate the value of r. In these plots the contribution of the operator $\mathrm{Re}(F_{D_1}^{\mathrm{dir}})$ dominates in the superposition $\mathrm{Re}(F_{D_1}^{\mathrm{dir}}) + H_B^* H_B$ as long as $R < r$ (i.e., $B \subseteq D_1$), while the contribution of the operator $H_B^* H_B$ dominates when $R > r$ (i.e., $D_1 \subseteq B$).
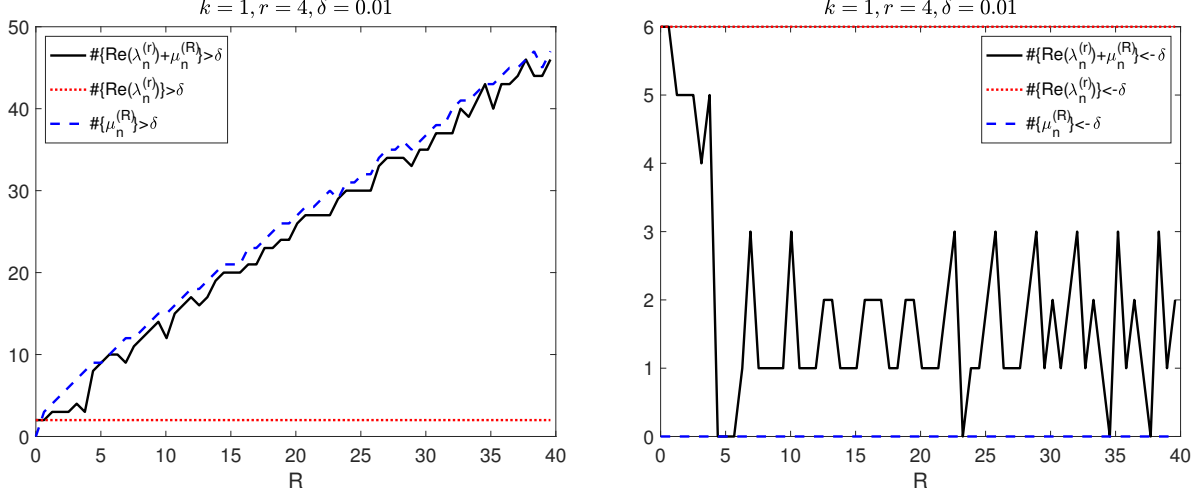
17

Figure 6.2: Same as Figure 6.1, but with $\delta = 0.01$ instead of $\delta = 0$.

Using asymptotic expansions for Bessel functions for large order (see [34, 11.19.1–2]) we find that

$$\mathrm{Re}(\lambda_n^{(r)}) = -4\pi\left(\frac{er}{2n}\right)^{2n} \qquad \text{and} \qquad \mu_n^{(R)} = 2\pi\frac{R}{n}\left(\frac{eR}{2n}\right)^{2n} \qquad \text{as } n \to \infty\,.$$

Accordingly, both sequences $(\mathrm{Re}(\lambda_n^{(r)}))_{n\in\mathbb{Z}}$ and $(\mu_n^{(R)})_{n\in\mathbb{Z}}$ decay rapidly once the value of $|n|$ is sufficiently large. Since eigenvalues below some threshold are rounded to zero in Matlab, and since the eigenvalues $\mu_n^{(R)}$ are on average increasing with respect to R, this explains the increasing but somewhat low numbers of positive eigenvalues of $H_B^* H_B$ in the left plot in Figure 6.1. A similar reasoning explains the seemingly low numbers of negative eigenvalues of $\mathrm{Re}(F_{D_1}^{\mathrm{dir}})$ in the right plot in Figure 6.1.

In practice the far field data will usually be corrupted by measurement errors, and it will not be possible to compute the eigenvalues of $\mathrm{Re}(F_{D_1}^{\mathrm{dir}}) + H_B^* H_B$ with very high precision, as done in this example so far. To see how this influences the numerical results, we repeat the previous computations but consider only those eigenvalues that are larger than a threshold $\delta = 0.01$. For comparison, we note that the largest eigenvalue of $\mathrm{Re}(F_{D_1}^{\mathrm{dir}})$ in this example is $\mathrm{Re}(\lambda_2^{(r)}) \approx 11.03$. In Figure 6.2 we show plots of the number of positive eigenvalues $\mathrm{Re}(\lambda_n^{(r)})$ (dotted), $\mu_n^{(R)}$ (dashed), and $\mathrm{Re}(\lambda_n^{(r)}) + \mu_n^{(R)}$ (solid) within the range $n = 0, \ldots, 1000$ that are larger than δ (left plot) and of the number of negative eigenvalues that are smaller than $-\delta$ (right plot) as a function of R. The transition in the behavior of the eigenvalues of $\mathrm{Re}(F_{D_1}^{\mathrm{dir}}) + H_B^* H_B$ at $R = r = 4$ is not nearly as pronounced as before. However, a rough estimate of r would still be possible by visual inspection of these plots, in particular from the plot on the right hand side of Figure 6.2.

6.2 A sampling strategy for Dirichlet or Neumann obstacles

In the special case, when only Dirichlet obstacles are present, the number of positive eigenvalues of $\mathrm{Re}(F_{D_1}^{\mathrm{dir}}) + H_B^* H_B$ can be utilized to decide whether a *probing domain* $B \subseteq \mathbb{R}^2$ is contained in the support of the scatterer D_1 or not. We discuss this approach in the following and comment on the special case, when only Neumann obstacles are present at the end of this section.

18

Let $D_2 = \emptyset$, and let $D_1 \subseteq \mathbb{R}^2$ be open and Lipschitz bounded. We assume that far field observations $u^\infty(\widehat{x}_l; \theta_m)$ are available for N equidistant observation and incident directions

$$\widehat{x}_l, \theta_m \in \{(\cos\phi_n, \sin\phi_n) \in S^1 \mid \phi_n = (n-1)2\pi/N, \ n = 0, \ldots, N-1\}, \tag{6.5}$$

$1 \leq l, m \leq N$. Accordingly, applying the trapezoid rule to (2.5), we find that the matrix

$$\boldsymbol{F}_{D_1}^{\mathrm{dir}} := \frac{2\pi}{N}[u^\infty(\widehat{x}_l; \theta_m)]_{1 \leq l,m \leq N} \in \mathbb{C}^{N \times N} \tag{6.6}$$

approximates the far field operator $F_{D_1}^{\mathrm{dir}}$. Assuming that the support of the scatterer D_1 is contained in the disk $B_R(0)$ for some $R > 0$, we require

$$N \gtrsim 2kR, \tag{6.7}$$

where as before k denotes the wave number, to fully resolve the relevant information contained in the far field patterns (see, e.g., [17]).

We consider an equidistant grid of points

$$\Delta = \{z_{ij} = (ih, jh) \mid -J \leq i, j \leq J\} \subseteq [-R, R]^2 \tag{6.8}$$

with step size $h = R/J$ in the region of interest $[-R, R]^2$. For each $z_{ij} \in \Delta$ we consider a *probing operator* $H_{B_{ij}}^* H_{B_{ij}}$ with $B_{ij} = B_{h/2}(z_{ij})$. Applying the trapezoid rule to (6.2) we find that for each $z_{ij} \in \Delta$ this operator is approximated by the matrix

$$\boldsymbol{T}_{B_{ij}} = \frac{2\pi}{N}\left[\pi h e^{\mathrm{i}kz_j \cdot (\theta_m - \theta_l)} J_0\left(\frac{kh}{2}|\theta_m - \theta_l|\right)\right]_{1 \leq l,m \leq N} \in \mathbb{C}^{N \times N}. \tag{6.9}$$

Therewith, we compute the eigenvalues $\lambda_1^{(ij)}, \ldots, \lambda_N^{(ij)} \in \mathbb{R}$ of the self-adjoint matrix

$$\boldsymbol{A}_{B_{ij}}^{\mathrm{dir}} = \mathrm{Re}(\boldsymbol{F}_{D_1}^{\mathrm{dir}}) + \boldsymbol{T}_{B_{ij}}, \qquad -J \leq i, j \leq J. \tag{6.10}$$

For numerical stabilization, we discard eigenvalues with absolute values smaller than some threshold. This threshold depends on the quality of the given far field data. If there are good reasons to believe that $\boldsymbol{A}_{B_{ij}}^{\mathrm{dir}}$ is known up to a perturbation of size $\delta > 0$ with respect to the spectral norm, then we can only trust in those eigenvalues with magnitude larger than δ (see, e.g., [15, Thm. 7.2.2]). To obtain a reasonable estimate for δ, we use the magnitude of the non-normal part of $\boldsymbol{F}_{D_1}^{\mathrm{dir}}$, i.e., we take $\delta = \|(\boldsymbol{F}_{D_1}^{\mathrm{dir}})^* \boldsymbol{F}_{D_1}^{\mathrm{dir}} - \boldsymbol{F}_{D_1}^{\mathrm{dir}}(\boldsymbol{F}_{D_1}^{\mathrm{dir}})^*\|_2$, since this quantity should be zero for exact data and be of the order of the data error, otherwise.

The characterization of the support of Dirichlet obstacles in Theorem 5.3 suggests that we count for each sampling point $z_{ij} \in \Delta$ the number of positive eigenvalues of $\boldsymbol{A}_{B_{ij}}^{\mathrm{dir}}$. We define the *indicator function* $I_{\mathrm{dir}} : \Delta \to \mathbb{N}$,

$$I_{\mathrm{dir}}(z_{ij}) = \#\{\lambda_n^{(ij)} \mid \lambda_n^{(ij)} > \delta, \ 1 \leq n \leq N\}, \qquad -J \leq i, j \leq J. \tag{6.11}$$

Theorem 5.3 suggests that I_{dir} admits smaller values at test points z_{ij} inside the obstacle than for test points outside of D_1.
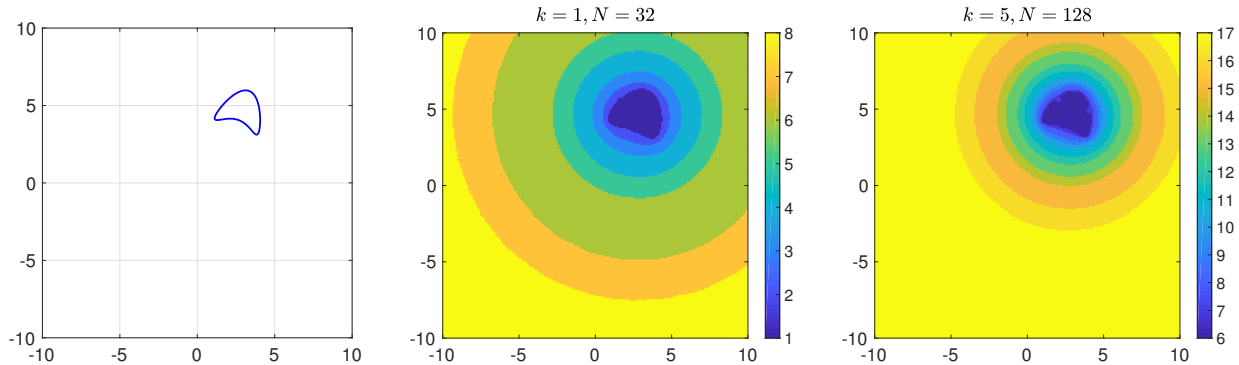
Figure 6.3: Exact shape of Dirichlet obstacle (left). Visualization of indicator function I_{dir} for two different wave numbers $k = 1$ with $N = 32$ (middle) and $k = 5$ with $N = 128$ (right).
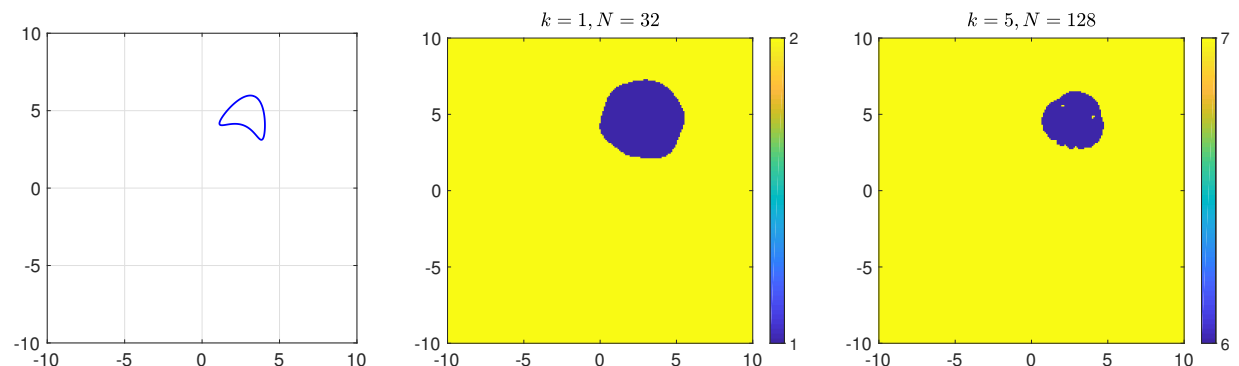

Figure 6.4: Same as in Figure 6.3, but with 0.1% complex-valued uniformly distributed error on far field data.

Example 6.1. We consider a single Dirichlet obstacle that has the shape of a kite as sketched in Figure 6.3 (left), and simulate the corresponding far field matrix $\boldsymbol{F}_{D_1}^{\mathrm{dir}} \in \mathbb{C}^{N \times N}$ for N observation and incident directions as in (6.5) using a Nyström method for a boundary integral formulation of the scattering problem (2.2) for two different wave numbers $k = 1$ (with $N = 32$), and for $k = 5$ (with $N = 128$) in accordance with the sampling condition (6.7).

In Figure 6.3 we show color coded plots of the indicator function I_{dir} from (6.11) with threshold parameter $\delta = 10^{-14}$ (i.e., the number of positive eigenvalues of the matrix $\boldsymbol{A}_{B_{ij}}^{\mathrm{dir}}$ from (6.10) that are larger than $\delta = 10^{-14}$ evaluated at each grid point $z_{ij} \in \Delta$) in the region of interest $[-10, 10]^2 \subseteq \mathbb{R}^2$. The sampling grid Δ from (6.8) consists of $2J + 1 = 201$ grid points in each direction.

The number of positive eigenvalues of the matrix $\boldsymbol{A}_{B_{ij}}^{\mathrm{dir}}$ increases with increasing wave number, and it is larger at test points z_{ij} sufficiently far away from the support of the scatterers than at test points z_{ij} inside, as suggested by Theorem 5.3. The lower value always coincides with the number of positive eigenvalues of the real part $\mathrm{Re}(\boldsymbol{F}_{D_1}^{\mathrm{dir}})$ of the far field matrix from (6.6) that are larger than the threshold δ. The total number of eigenvalues of $\boldsymbol{A}_{B_{ij}}^{\mathrm{dir}}$, $j = 1, \ldots, J$, whose absolute values are larger than δ is approximately (on average over all grid points) 24 (for $k = 1$) and 50 (for $k = 5$).

Depending on the wave number, the lowest level set of the indicator function I_{dir} nicely approximates the support of the scatterer.

The reconstruction algorithm is rather sensitive to noise in the far field data. To see this, we
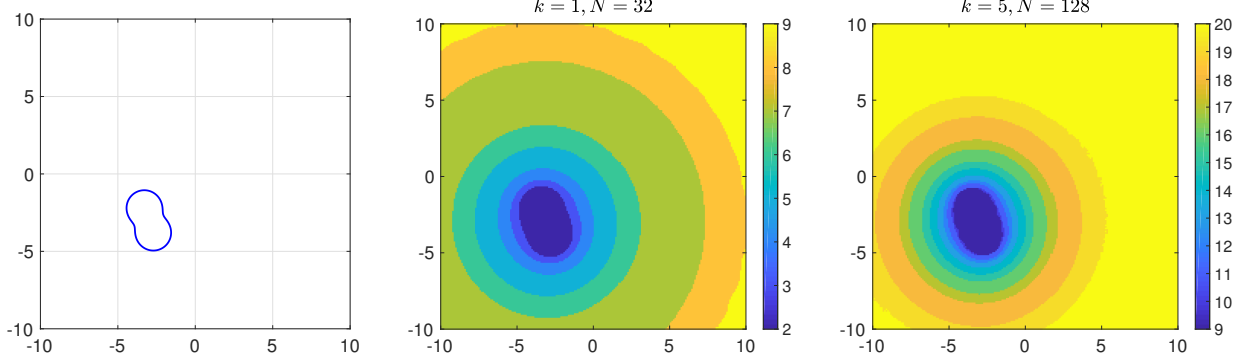
20

Figure 6.5: Exact shape of Neumann obstacle (left). Visualization of indicator function I_{neu} for two different wave numbers $k = 1$ with $N = 32$ (middle), and $k = 5$ with $N = 128$ (right).

repeat the previous computation but add 0.1% complex-valued uniformly distributed error to the far field matrix $\boldsymbol{F}_{D_1}^{\text{dir}}$ that we simulate using the Nyström method. We estimate the non-normality error of the corresponding scattering operator and accordingly we choose $\delta = 0.1$ for the threshold in the reconstruction algorithm. In Figure 6.4, we show color coded plots of the indicator function I_{dir} from (6.11) for wave numbers $k = 1$ (with $N = 32$), and for $k = 5$ (with $N = 128$). The total number of eigenvalues of $\boldsymbol{A}_{B_{ij}}^{\text{dir}}$, $j = 1, \ldots, J$, whose absolute values are larger than δ is approximately (on average over all grid points) 8 (for $k = 1$) and 22 (for $k = 5$).

The reconstruction for $k = 5$ is better than the reconstruction for $k = 1$ because more eigenvectors are stably propagated into the far field for larger wave numbers (the number of eigenvalues with absolute values above the threshold δ increases with k). However, despite the low noise level, the shape of the obstacle is not reconstructed very well. $\diamond$

If only Neumann obstacles are present, i.e., $D_1 = \emptyset$ and $D_2 \subseteq \mathbb{R}^2$ is open and Lipschitz bounded, then we use the corresponding far field matrix $\boldsymbol{F}_{D_2}^{\text{neu}} \in \mathbb{C}^{N \times N}$ as in (6.6) and the matrix $\boldsymbol{T}_{B_{ij}} \in \mathbb{C}^{N \times N}$ from (6.9) to compute for each sampling point $z_{ij} \in \Delta$ the eigenvalues $\lambda_1^{(ij)}, \ldots, \lambda_N^{(ij)} \in \mathbb{R}$ of the self-adjoint matrix

$$\boldsymbol{A}_{B_{ij}}^{\text{neu}} = -\left(\text{Re}(\boldsymbol{F}_{D_2}^{\text{neu}}) - \boldsymbol{T}_{B_{ij}}\right), \qquad -J \leq i, j \leq J.$$

The characterization of the support of Neumann obstacles in Theorem 5.4 suggests that we count for each sampling point $z_{ij} \in \Delta$ the number of positive eigenvalues of $\boldsymbol{A}_{B_{ij}}^{\text{neu}}$. We define the *indicator function* $I_{\text{neu}} : \Delta \to \mathbb{N}$,

$$I_{\text{neu}}(z_{ij}) = \#\{\lambda_n^{(ij)} \mid \lambda_n^{(ij)} > \delta, \ 1 \leq n \leq N\}, \qquad -J \leq i, j \leq J. \qquad (6.12)$$

Theorem 5.4 suggests that I_{neu} admits smaller values at test points z_{ij} inside the obstacle than for test points outside of D_2.

Example 6.2. In the second example, we consider a Neumann obstacle that has the shape of a peanut as sketched in Figure 6.5. We simulate the corresponding far field matrix $\boldsymbol{F}_{D_2}^{\text{neu}} \in \mathbb{C}^{N \times N}$ for N observation and incident directions using a Nyström method for a boundary integral formulation of the scattering problem (2.2) for two different wave numbers $k = 1$ (with $N = 32$), and for $k = 5$ (with $N = 128$).

21

In Figure 6.5 we show color coded plots of the indicator function I_{neu} from (6.12) with threshold parameter $\delta = 10^{-14}$ in the region of interest $[-10,10]^2 \subseteq \mathbb{R}^2$. The equidistant rectangular sampling grid on the region of interest from (6.8) consists of 201 grid points in each direction.

Again, the number of positive eigenvalues of the matrix $\boldsymbol{A}_{B_{ij}}$ increases with increasing wave number, and it is larger at test points z_{ij} sufficiently far away from the support of the scatterers than at test points z_{ij} inside, in compliance with Theorem 5.4. The lower value always coincides with the number of negative eigenvalues of the matrix $\mathrm{Re}(\boldsymbol{F}_{D_2}^{\mathrm{neu}})$ that are smaller than the threshold $-\delta = -10^{-14}$. The number of eigenvalues of $\boldsymbol{A}_{B_{ij}}^{\mathrm{neu}}$, $j = 1, \ldots, J$, whose absolute values are larger than $\delta = 10^{-14}$ is approximately (on average over all grid points) 25 (for $k = 1$) and 55 (for $k = 5$).

Depending on the wave number the support of the indicator function I_{neu} approximates the support of the scatterer rather well. $\diamondsuit$

6.3 Separating mixed obstacles

We return to the general mixed case, i.e., when both Dirichlet and Neumann obstacles are present. While the algorithm developed for Dirichlet or Neumann obstacles in the previous subsection determines whether a sufficiently small probing domain B is contained inside the support of the unknown scattering obstacle D or not, the shape characterization for mixed obstacles established in Theorem 5.5 describes whether a sufficiently large probing domain B contains the support D of the scattering objects or not. A corresponding numerical algorithm that implements a similar criterion for the inverse conductivity problem has recently been proposed in [13]. However, since in contrast to the inverse conductivity problem, the monotonicity relations in Theorem 5.5 only hold up to certain finite dimensional subspaces of unknown dimension, an extension of the reconstruction algorithm from [13] to the mixed inverse obstacle problem is not straightforward.

In the following we consider a reduced problem, and utilize Theorem 5.5 to develop an algorithm to recover the convex hulls of the Dirichlet obstacle D_1 and of the Neumann obstacle D_2 separately. We treat the Dirichlet part first, and comment on the Neumann part below. The idea is to consider a sufficiently large number of probing disks $B = B_R(z) \subseteq \mathbb{R}^2$, where for each center $z \in \mathbb{R}^2$ the radius $R > 0$ is chosen as small as possible but such that B still completely covers D_1. Intersecting those disks then gives an approximation of the convex hull of D_1. To determine the optimal radius R for each of these disks, we use Theorem 5.5, which (under some additional assumptions) says that

(a) if $\overline{D_1} \subseteq B$, then $\mathrm{Re}(F_D^{\mathrm{mix}}) + H_B^* H_B$ has only finitely many negative eigenvalues, and

(b) if $D_1 \not\subseteq B$, then $\mathrm{Re}(F_D^{\mathrm{mix}}) + H_B^* H_B$ has infinitely many negative eigenvalues.

Example 6.3. We consider a kite-shaped Dirichlet obstacle and a peanut-shaped Neumann obstacle as shown in Figure 6.6 (left). We simulate the corresponding far field matrix $\boldsymbol{F}_D^{\mathrm{mix}} \in \mathbb{C}^{N \times N}$ analogous to (6.6) for wave number $k = 1$ and $N = 64$ observation and incident directions using a Nyström method for a boundary integral formulation of the mixed scattering problem (2.2).

To begin with, we fix the center $z = (15, 0)$ of a single probing disk $B = B_R(z)$ and evaluate the matrix

$$\boldsymbol{A}_{B_R(z)}^{\mathrm{mix},+} = \mathrm{Re}(\boldsymbol{F}_D^{\mathrm{mix}}) + \boldsymbol{T}_{B_R(z)}$$

on a whole interval of radii $0 < R < 40$. Here the matrix $\boldsymbol{T}_{B_R(z)} \in \mathbb{C}^{N \times N}$ is defined analogous to (6.9). As in our previous examples we choose a threshold parameter $\delta = 10^{-14}$, and in Figure 6.6
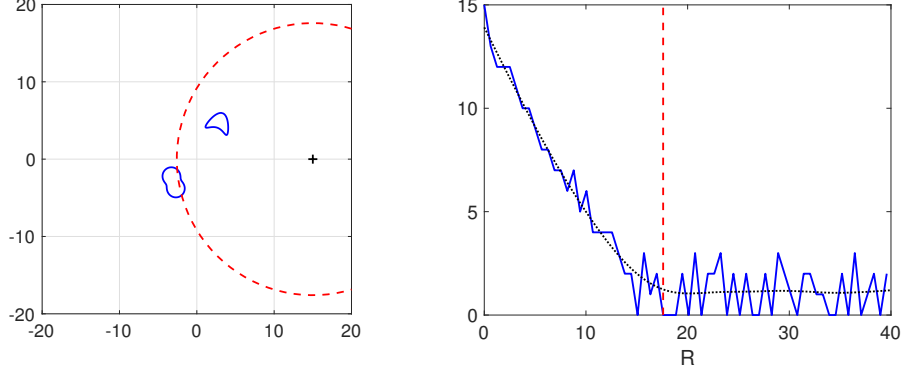
Figure 6.6: Left: Exact shape of mixed obstacles (solid), smallest disk around $z = (15,0)$ containing the Dirichlet obstacle (dashed). Right: Number of negative eigenvalues of $\boldsymbol{A}_{B_R(z)}^{\mathrm{mix},+}$ smaller than $-\delta = -10^{-14}$ as function of radius R (solid), smoothing spline (dotted), estimated radius of smallest disk around $z = (15,0)$ containing Dirichlet obstacle (dashed).

(right) we show the number of negative eigenvalues of $\boldsymbol{A}_{B_R(z)}^{\mathrm{mix},+}$ that are smaller than $-\delta$ as a function of the radius R (solid).

We observe a similar behavior as for the concentric disks studied in Section 6.1 (cf. the plots on the right hand side of Figures 6.1 and 6.2). The number of negative eigenvalues of $\boldsymbol{A}_{B_R(z)}^{\mathrm{mix},+}$ decreases with increasing R until it becomes stationary up to small oscillations around $R \approx 18$. Our theoretical results suggest that radius R, where this transition from decreasing to almost stationary appears, corresponds to the radius of the smallest disk that still completely covers the Dirichlet obstacle D_1.

To evaluate this transition numerically, we fit a smoothing spline curve through the number of negative eigenvalues of $\boldsymbol{A}_{B_R(z)}^{\mathrm{mix},+}$ as shown on the right hand side of Figure 6.6 (dotted). We determine the point of maximum signed curvature of this smoothing spline and use the corresponding value of R as approximation of the radius of the smallest disk around z that still completely covers the Dirichlet obstacle D_1. On the right hand side of Figure 6.6 the result of this strategy is shown as a dashed vertical line, and the corresponding disk $B_R(z)$ is shown on the left hand side of Figure 6.6 (dashed). $\diamondsuit$

Similarly, for the Neumann obstacle Theorem 5.5 says that

(c) if $\overline{D_2} \subseteq B$, then $-(\mathrm{Re}(F_D^{\mathrm{mix}}) - H_B^* H_B)$ has only finitely many negative eigenvalues, and

(d) if $D_2 \not\subseteq B$, then $-(\mathrm{Re}(F_D^{\mathrm{mix}}) - H_B^* H_B)$ has infinitely many negative eigenvalues.

Introducing

$$\boldsymbol{A}_{B_R(z)}^{\mathrm{mix},-} = -\big(\mathrm{Re}(\boldsymbol{F}_D^{\mathrm{mix}}) - \boldsymbol{T}_{B_R(z)}\big)$$

we can proceed as in Example 6.3 for the Dirichlet obstacle to determine minimal radii of probing disks $B_R(z)$ containing the Neumann obstacle.

Example 6.4. We continue with Example 6.3 and pick 16 evenly spaced points $z_1, \ldots, z_{16}$ on a circle of radius 15 around the origin, which are shown as solid pluses in the two plots on the right hand side of Figure 6.7. The points z_ℓ, $\ell = 1, \ldots, 16$, are the centers of 16 probing disks that are used to approximate the convex hulls of the Dirichlet obstacle and of the Neumann obstacle separately.
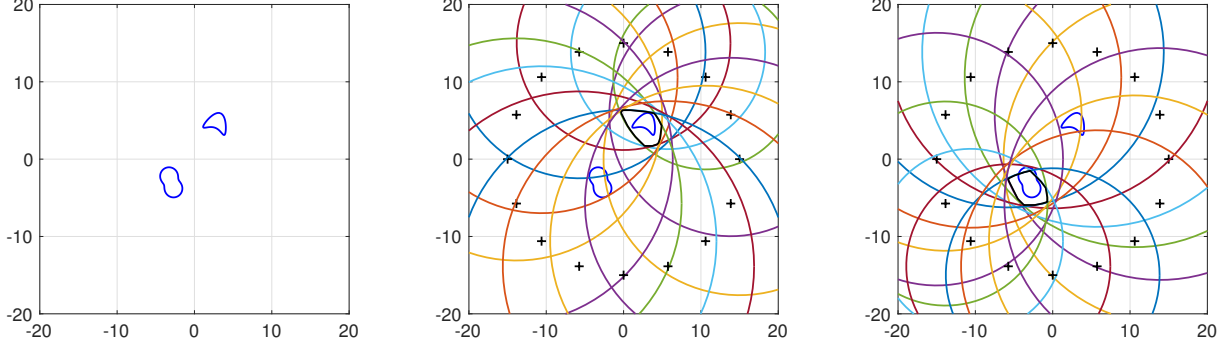
23

Figure 6.7: Exact shape of mixed obstacles (left). Visualization of reconstructions of convex hulls of Dirichlet obstacle (middle) and of Neumann obstacle (right) for $k = 1$ (with $N = 64$).
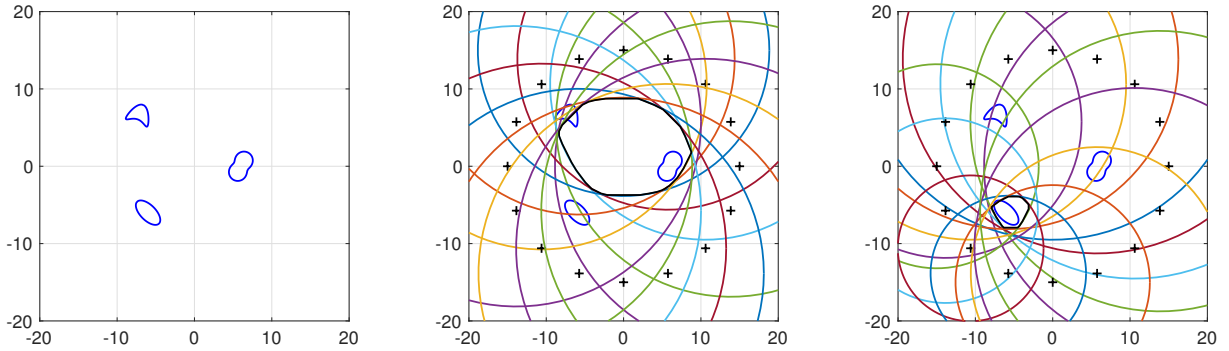

Figure 6.8: Same as Figure 6.7 but with three obstacles.

For each center z_ℓ we estimate the radii R_ℓ^{dir} and R_ℓ^{neu} of the smallest disks $B_{R_\ell^{\mathrm{dir}}}(z_\ell)$ and $B_{R_\ell^{\mathrm{neu}}}(z_\ell)$ centered at z_ℓ that completely cover the Dirichlet obstacle and the Neumann obstacle, respectively. These estimates are obtained as described in Example 6.3. Therewith we compute approximations

$$\mathscr{C}^{\mathrm{dir}} = \bigcap_{\ell=1}^{16} B_{R_\ell^{\mathrm{dir}}}(z_\ell) \qquad \text{and} \qquad \mathscr{C}^{\mathrm{neu}} = \bigcap_{\ell=1}^{16} B_{R_\ell^{\mathrm{neu}}}(z_\ell)$$

of the convex hulls of D_1 and of D_2, respectively. The results are shown in Figure 6.7 (middle and right). ◊

Example 6.5. We consider another example with two Dirichlet obstacles (kite-shaped and peanut-shaped) and one Neumann obstacle (an ellipse) as shown in Figure 6.8 (left). We simulate the corresponding far field matrix $\boldsymbol{F}_D^{\mathrm{mix}} \in \mathbb{C}^{N \times N}$ for wave number $k = 1$ and $N = 64$ observation and incident directions using a Nyström method, and we apply the reconstruction scheme to approximate the convex hulls of the Dirichlet obstacles D_1 and of the Neumann obstacles D_2 with the same parameters as in the previous example. The reconstructions $\mathscr{C}^{\mathrm{dir}}$ and $\mathscr{C}^{\mathrm{neu}}$ are shown in Figure 6.8 (middle and right). ◊

Further numerical experiments show that this algorithm is also very sensitive to noise in the data.

24

Conclusions

Locating and estimating the shape of scatterers based on far field observations is a basic problem in remote sensing. In this work we have established a monotonicity based shape characterization for a mixed inverse obstacle scattering problem. Using this technique we have shown that the shape of Dirichlet and Neumann obstacles are uniquely determined independently by the corresponding far field operator without additional a priori information. Numerical examples have been presented to illustrate the potential and limitations of applications of these theoretical results in reconstruction algorithms. However, the question of how to apply the novel monotonicity principles in an efficient and robust shape reconstruction algorithm for mixed inverse obstacle problems requires further research efforts.

Acknowledgments

References

[1] A. Barth, B. Harrach, N. Hyvönen, and L. Mustonen. Detecting stochastic inclusions in electrical impedance tomography. *Inverse Problems*, 33(11):115012, 18, 2017.

[2] T. Brander, B. Harrach, M. Kar, and M. Salo. Monotonicity and enclosure methods for the p-Laplace equation. *SIAM J. Appl. Math.*, 78(2):742–758, 2018.

[3] F. Cakoni and D. Colton. *A qualitative approach to inverse scattering theory*, volume 188 of *Applied Mathematical Sciences*. Springer, New York, 2014.

[4] F. Cakoni, D. Colton, and P. Monk. The direct and inverse scattering problems for partially coated obstacles. *Inverse Problems*, 17(6):1997–2015, 2001.

[5] F. Cakoni, D. Colton, and P. Monk. The electromagnetic inverse-scattering problem for partly coated Lipschitz domains. *Proc. Roy. Soc. Edinburgh Sect. A*, 134(4):661–682, 2004.

[6] F. Cakoni, D. Colton, and P. Monk. *The linear sampling method in inverse electromagnetic scattering*, volume 80 of *CBMS-NSF Regional Conference Series in Applied Mathematics*. Society for Industrial and Applied Mathematics (SIAM), Philadelphia, PA, 2011.

[7] V. Candiani, J. Dardé, H. Garde, and N. Hyvönen. Monotonicity-based reconstruction of extreme inclusions in electrical impedance tomography. *arXiv preprint arXiv:1909.12110*, 2019.

[8] D. Colton and A. Kirsch. A simple method for solving inverse scattering problems in the resonance region. *Inverse Problems*, 12(4):383–393, 1996.

[9] D. Colton and R. Kress. *Inverse acoustic and electromagnetic scattering theory*, volume 93 of *Applied Mathematical Sciences*. Springer, New York, third edition, 2013.

[10] T. Daimon, T. Furuya, and R. Saiin. The monotonicity based method for the inverse crack scattering problem. *arXiv preprint arXiv:1904.03655*, 2019.

[11] H. Garde. Comparison of linear and non-linear monotonicity-based shape reconstruction using exact matrix characterizations. *Inverse Probl. Sci. Eng.*, 26(1):33–50, 2018.

[12] H. Garde and S. Staboulis. Convergence and regularization for monotonicity-based shape reconstruction in electrical impedance tomography. *Numer. Math.*, 135(4):1221–1251, 2017.

[13] H. Garde and S. Staboulis. The regularized monotonicity method: detecting irregular indefinite inclusions. *Inverse Probl. Imaging*, 13(1):93–116, 2019.

[14] B. Gebauer. Localized potentials in electrical impedance tomography. *Inverse Probl. Imaging*, 2(2):251–269, 2008.

[15] G. H. Golub and C. F. Van Loan. *Matrix computations*. Johns Hopkins Studies in the Mathematical Sciences. Johns Hopkins University Press, Baltimore, MD, fourth edition, 2013.

[16] R. Griesmaier and B. Harrach. Monotonicity in inverse medium scattering on unbounded domains. *SIAM J. Appl. Math.*, 78(5):2533–2557, 2018.

[17] R. Griesmaier and J. Sylvester. Uncertainty principles for inverse source problems, far field splitting, and data completion. *SIAM J. Appl. Math.*, 77(1):154–180, 2017.

[18] N. I. Grinberg. Obstacle visualization via the factorization method for the mixed boundary value problem. *Inverse Problems*, 18(6):1687–1704, 2002.

[19] N. I. Grinberg and A. Kirsch. The factorization method for obstacles with a priori separated sound-soft and sound-hard parts. *Math. Comput. Simulation*, 66(4-5):267–279, 2004.

[20] B. Harrach and Y.-H. Lin. Monotonicity-based inversion of the fractional Schrödinger equation I. Positive potentials. *SIAM J. Math. Anal.*, 51(4):3092–3111, 2019.

[21] B. Harrach and Y.-H. Lin. Monotonicity-Based Inversion of the Fractional Schödinger Equation II. General Potentials and Stability. *SIAM J. Math. Anal.*, 52(1):402–436, 2020.

[22] B. Harrach and M. N. Minh. Enhancing residual-based techniques with shape reconstruction features in electrical impedance tomography. *Inverse Problems*, 32(12):125002, 21, 2016.

[23] B. Harrach and M. N. Minh. Monotonicity-based regularization for phantom experiment data in electrical impedance tomography. In *New trends in parameter identification for mathematical models*, Trends Math., pages 107–120. Birkhäuser/Springer, Cham, 2018.

[24] B. Harrach, V. Pohjola, and M. Salo. Dimension Bounds in Monotonicity Methods for the Helmholtz Equation. *SIAM J. Math. Anal.*, 51(4):2995–3019, 2019.

[25] B. Harrach, V. Pohjola, and M. Salo. Monotonicity and local uniqueness for the Helmholtz equation. *Anal. PDE*, 12(7):1741–1771, 2019.

[26] B. Harrach and M. Ullrich. Monotonicity-based shape reconstruction in electrical impedance tomography. *SIAM J. Math. Anal.*, 45(6):3382–3403, 2013.

[27] B. Harrach and M. Ullrich. Resolution guarantees in electrical impedance tomography. *IEEE transactions on medical imaging*, 34(7):1513–1521, 2015.

[28] M. Ikehata. Size estimation of inclusion. *J. Inverse Ill-Posed Probl.*, 6(2):127–140, 1998.

[29] H. Kang, J. K. Seo, and D. Sheen. The inverse conductivity problem with one measurement: stability and estimation of size. *SIAM J. Math. Anal.*, 28(6):1389–1405, 1997.

[30] A. Kirsch. Characterization of the shape of a scattering obstacle using the spectral data of the far field operator. *Inverse Problems*, 14(6):1489–1512, 1998.

[31] A. Kirsch and N. Grinberg. *The factorization method for inverse problems*, volume 36 of *Oxford Lecture Series in Mathematics and its Applications*. Oxford University Press, Oxford, 2008.

[32] A. Maffucci, A. Vento, S. Ventre, and A. Tamburrino. A novel technique for evaluating the effective permittivity of inhomogeneous interconnects based on the monotonicity property. *IEEE Transactions on Components, Packaging and Manufacturing Technology*, 6(9):1417–1427, 2016.

[33] W. McLean. *Strongly elliptic systems and boundary integral equations*. Cambridge University Press, Cambridge, 2000.

[34] F. W. J. Olver, D. W. Lozier, R. F. Boisvert, and C. W. Clark, editors. *NIST handbook of mathematical functions*. U.S. Department of Commerce, National Institute of Standards and Technology, Washington, DC; Cambridge University Press, Cambridge, 2010. With 1 CD-ROM (Windows, Macintosh and UNIX).

[35] R. Potthast. A survey on sampling and probe methods for inverse problems. *Inverse Problems*, 22(2):R1–R47, 2006.

[36] Z. Su, L. Udpa, G. Giovinco, S. Ventre, and A. Tamburrino. Monotonicity principle in pulsed eddy current testing and its application to defect sizing. In *Applied Computational Electromagnetics Society Symposium-Italy (ACES), 2017 International*, pages 1–2. IEEE, 2017.

[37] A. Tamburrino and G. Rubinacci. A new non-iterative inversion method for electrical resistance tomography. *Inverse Problems*, 18(6):1809–1829, 2002. Special section on electromagnetic and ultrasonic nondestructive evaluation.

[38] A. Tamburrino, Z. Sua, S. Ventre, L. Udpa, and S. S. Udpa. Monotonicity based imaging method in time domain eddy current testing. *Electromagnetic Nondestructive Evaluation (XIX)*, 41:1, 2016.